JUL 15 1959 RECEIVED

For presentation at SAS National Summer Meeting, June 16-19, 1959, Los Angeles, Calif.

DESIGN OF ION ROCKETS AND TEST FACILITIES

By J. H. Childs

Lewis Research Center
National Aeronautics and Space Administration
Cleveland, Ohio

N65-82417
Code Doxe
(Nasa TM X-56111

INTRODUCTION

The great interest in ion rockets stems, of course, from their potential for supplying extremely high values of specific impulse. Chemical rockets are limited to values of specific impulse in the neighborhood of 400 sec by the available chemical enthalpy in the propellants. Nuclear thermal rockets are limited to a specific impulse around 800 sec by materials limitations. But ion rockets can provide a specific impulse of 10,000 sec or even higher if desired. Although the powerplant required to generate the electric power is quite heavy, ion rockets nevertheless offer over-all weight savings when compared with the lower-specific-impulse propulsion systems for many space missions.

For each mission there is some optimum specific impulse that results in the lowest combined powerplant and propellant weight. For nuclear turboelectric power systems and for reasonable extrapolations of current technology, it appears that a thrust-weight ratio of about 10^{-4} g's can be achieved and a specific impulse of 10,000 sec is about optimum for a round-trip Mars mission (ref. 1). Longer missions require higher values of specific impulse; advances in technology to permit lighter powerplants will also result in a need for higher values of specific impulse.

Copy No. (1)
W
L
E
A
H

NASA FILE COPY
Loan expires on last date stamped on back cover.
PLEASE RETURN TO
DIVISION OF RESEARCH INFORMATION
NATIONAL AERONAUTICS
AND SPACE ADMINISTRATION
Washington 25, D. C.

Relatively low values of specific impulse may also be of interest for orbit adjustment on satellites. For short propulsion time and high powerplant specific weight, the optimum specific impulse may be as low as 1000 seconds if ion rocket efficiency is assumed to be independent of specific impulse; this assumption is not realistic, as discussed herein.

This paper reviews the performance characteristics of ion rockets with a view to assessing the level of efficiency that might ultimately be attained with these engines. The theoretical performance is considered for values of specific impulse from 1000 to 25,000 seconds.

The components of any ion rocket are a propellant supply system, an ion source, an ion accelerator, and an electron emitter. Considerable design data are available for each of these components due to the many fundamental studies of ionization phenomena and the many prior developments of electron guns and ion sources for mass spectrographs and particle accelerators. These data are reviewed to show how they provide design criteria for ion rockets. However, a practical ion rocket requires a high efficiency, small weight, and long operating life; these factors were not of such great importance in most of the prior developments noted above. Thus, much additional data must be obtained before a high-performance ion rocket can be developed. The research program of the NASA Lewis Research Center is described to indicate how we are attempting to obtain the necessary design data.

Finally, the research facilities necessary for ion rocket development are described. The theoretical considerations in the design

of ultra-high vacuum condenser tanks are reviewed, and some preliminary experimental data on tank performance are included.

PERFORMANCE CHARACTERISTICS

The performance of an ion rocket can be determined from the equations which follow. All symbols are defined in appendix A.

Ion beam current. -

$$I_B = \dot{m}_i \frac{\epsilon}{\mu_i} \tag{1}$$

Thrust. -

$$F = \frac{\dot{m}_i}{g} v_i + \frac{\dot{m}_e}{g} v_e \approx \frac{\dot{m}_i}{g} v_i = \frac{I_B}{g} \frac{\mu_i}{\epsilon} v_i \tag{2}$$

Exhaust velocity. - Conservation of energy, $\frac{1}{2} \mu_i v_i^2 = \epsilon U$ or,

$$v_i = 1.414 \sqrt{\frac{\epsilon}{\mu_i} U} \tag{3}$$

Power input. -

$$P_B = \frac{10^{-3}}{2} \dot{m}_i v_i^2 = 10^{-3} I_B U = 10^{-3} \dot{m}_i \frac{\epsilon}{\mu_i} U \tag{4}$$

Saturation beam current. - Due to space charge effects there exists a limiting, or saturation value, of ion beam current. Consider the simple case where ions are emitted from a plane surface at potential U and are accelerated toward another parallel plane at zero potential a distance L away. This parallel-plane diode is very similar to some ion engine configurations being given serious consideration; simplified diagrams of two such engines are shown in figure 1. The saturation current density, where $d\Phi/dx = 0$ at the ion emitter, is given by the relation (ref. 2):

$$i_s = 5.56 \times 10^{-12} \sqrt{\frac{\epsilon}{\mu}} \frac{U^{3/2}}{L^2} \tag{5}$$

Since the optimum value of I_{sp}, and hence v_i, is fixed by overall craft weight and mission considerations, it will prove convenient in the later discussion to express most of the other performance parameters in terms of v_i. If we do this for i_s, from equations (5) and (3) we get

$$i_s = 1.97\times10^{-12}\left(\frac{\mu}{\epsilon}\right)\frac{v_i^3}{L^2} \qquad (6)$$

The derivation of equations (5) and (6) assumed the ion velocity to be zero as they leave the ion source. This would obviously lead to a physically unrealizable infinite space charge density at the source. In practice, the initial ion velocity will not be zero, and the individual ion velocities will have a Maxwellian distribution. I. Langmuir has shown that for this case

$$\frac{i_{s,v_o}}{i_s} = 1 + 0.0247\sqrt{\frac{T}{U}} \qquad (7)$$

where i_{s,v_o} is the saturation current density with finite initial velocity and i_s is the current density obtained from equation (5) or (6). Thus, for the high accelerator voltages to be employed with heavy ions such as cesium, the effect of initial thermal velocities is almost nil, and the saturation current given by equations (5) and (6) is essentially correct.

If very light-weight ions such as hydrogen should ever be used as propellant, then we should modify equations (5) and (6) as required. Similarly, in the elctron guns, we must allow for initial-velocity effects on current density.

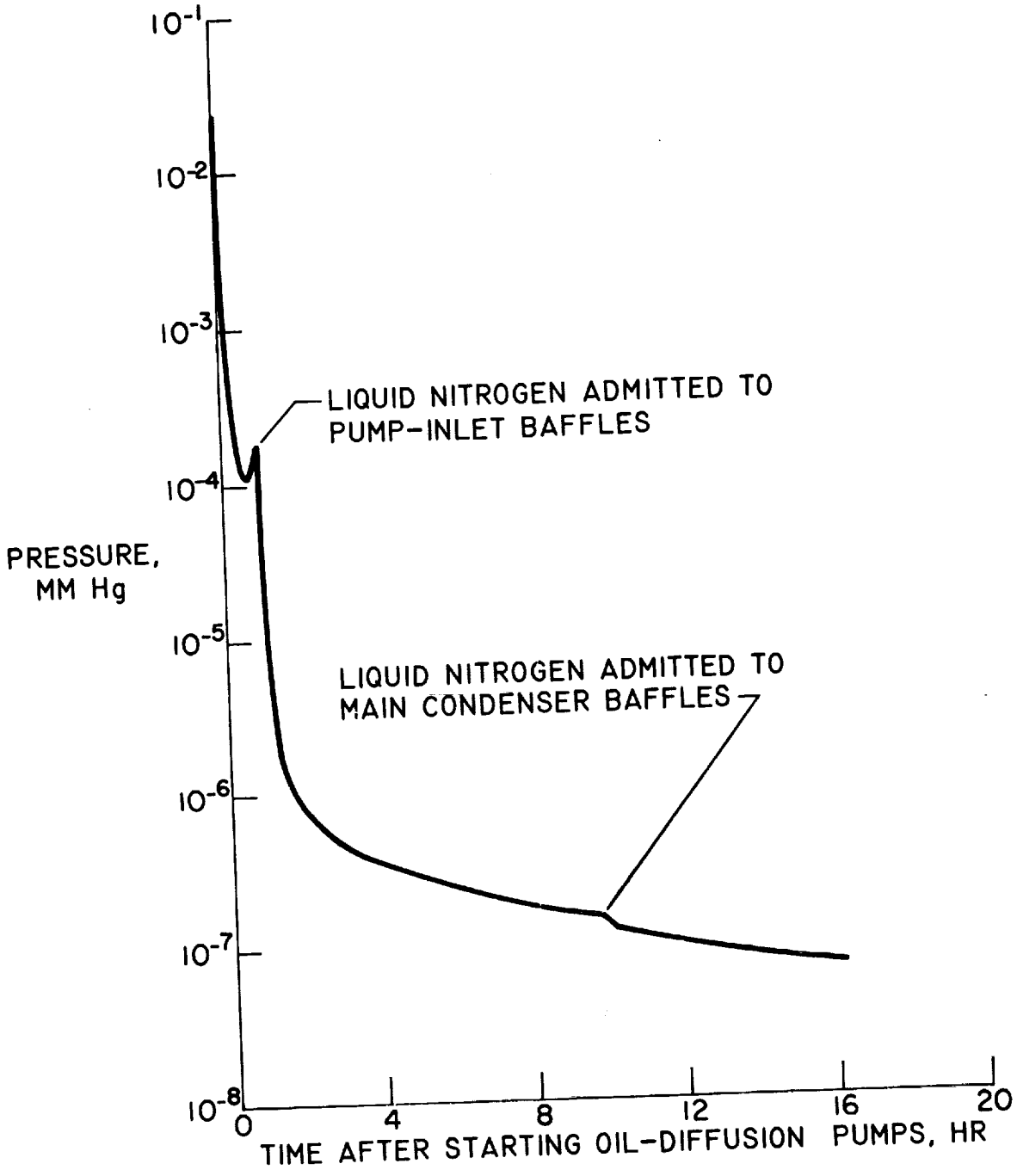

Figure 24. - Typical pressure-time history with no engine inside tank.

Thrust per unit area. - Maximum obtainable values are limited by space charge effects. From (2), (3), and (5),

$$\frac{F}{A} = 8\times10^{-13}\left(\frac{U}{L}\right)^2 = 8\times10^{-13}\,\overline{E}^2 \tag{8}$$

From (2) and (6),

$$\frac{F}{A} = 2\times10^{-13}\left(\frac{\mu}{\epsilon}\right)^2\frac{v^4}{L^2} \tag{9}$$

E-453

Power per unit area. - From (4) and (5),

$$\frac{P}{A} = 5.56\times10^{-15}\sqrt{\frac{\epsilon}{\mu}}\,\frac{U^{5/2}}{L^2} \tag{10}$$

From (4) and (6),

$$\frac{P}{A} = 9.85\times10^{-16}\left(\frac{\mu}{\epsilon}\right)^2\frac{v^5}{L^2} \tag{11}$$

Performance charts. - Figures 2 to 5 show the more important performance parameters on charts. The required accelerating voltages for ions and electrons appear in figures 2 and 3, respectively. Figure 4 shows the very large amounts of power required to produce even a few kilograms of thrust; this, of course, is inherent in any high-specific-impulse device. Figure 5 shows the power, thrust, and beam current per unit engine area.

PROPELLANTS

Most of the promising ion rocket propellants will be formed into single-atom, singly-charged ions in the ion source. Let us examine the effect that variations in atomic weight μ might have on the ion rocket design and performance. Since the considerations that lead to selection of the optimum exhaust velocity are only affected by

propellant properties in a very secondary manner, we can assume in this part of our discussion that we desire the same values of v_i and F for all propellants. Then,

$$F \propto \dot{m}_i v_i = n\mu A v_i^2 = i \frac{\mu}{\epsilon} Av = I \frac{\mu}{\epsilon} v$$

So, for fixed F and v_i,

$$I_1 \mu_1 = I_2 \mu_2 \tag{12}$$

From (6), for fixed v_i,

$$i_s = \frac{I}{A} \propto \frac{\mu}{L^2} \tag{13}$$

From (3), for fixed v_i,

$$U \propto \mu \tag{14}$$

Using these simplified relations we can quickly obtain relative values of the important design and performance criteria for two hypothetical propellants, with one having twice the atomic weight of the other. The following table shows the values computed for the case of an ion rocket designed for high specific impulse (e.g., 25,000 sec):

Performance parameters	Relative values for equal v and F		
Case	1(a)	1(b)	2
μ	1	1	2
I	2	2	1
A	1	2	1
i	2	1	1
L	$1/\sqrt{2}$	1	$\sqrt{2}$
U	1	1	2
$\overline{E} = U/L$	$\sqrt{2}$	1	$\sqrt{2}$
P	1	1	1

For the low-μ propellant, we have computed two cases: one having the same accelerator area (case 1(a)) as for the high-μ propellant, and one

having twice this area (case 1(b)). The comparison shows that, in terms of the over-all performance considerations listed in the table, there is no advantage in either a high-μ or a low-μ propellant: Although the low-μ case requires higher i if A is made the same, we can attain this i with the same value of $\overline{E}$ as for the high-μ propellant. Electrical breakdown between the high- and low-voltage electrodes is assumed to be the factor setting a minimum limit on L and hence a maximum attainable value on i. This electrical breakdown is primarily a function of E; therefore, since the required E is the same in cases 1(a) and 2 in the above table, it appears quite feasible to attain high F/A with either high-μ or low-μ propellants.

How, let us repeat this comparison for the case of an ion rocket designed for low specific impulse (e.g., 3000 sec).

Performance parameters	Relative values for equal v and F	
μ	1	2
I	2	1
L	1	1
i	1	2
A	1	1/4
U	1	2
$\overline{E} = U/L$	1	2
P	1	1

Here we make the realistic assumption (for this case) that the electrode spacing L is fixed by manufacturing tolerances, thermal distortion effects, etc. Thus, the minimum possible L is attainable with even the high-μ propellants. In this case, then, the required accelerator area increases inversely as the square of propellant atomic weight.

As will be subsequently discussed, the propellant atomic weight can also affect the efficiency of the ion rocket with higher μ permitting somewhat higher efficiency. In general, then, it can be stated that high propellant atomic weight may have some moderate advantage for high-specific-impulse ion rockets, and high atomic weight is mandatory for low-specific-impulse ion rockets.

The energy required to ionize the propellant is so small in comparison with that required to accelerate the ions that these differences between various propellants are not significant unless low-specific-impulse ion rockets using low-atomic-weight propellants are considered. Ionization potential is nevertheless important in most cases because it affects the ionization efficiency (ratio of ions to total particles leaving ion source). It is especially important where the surface ionization method is used; here, at best, the work function of the ionizing surface is only marginally above the ionization potential of the propellant. The alkali metals, which have very low ionization potentials, are the only materials known to be subject to surface ionization to any appreciable extent. Thus they are of considerable interest as propellants.

COMPONENT DESIGN AND PERFORMANCE

The major ion rocket components are:

1. Propellant supply system
2. Ion source
3. Ion accelerator
4. Electron emitter

The design principles for each of these components will be briefly reviewed, and where possible, an indication will be given of the performance to be expected from the individual components.

Propellant Supply Systems

Since the propellant flow rates are quite low, a gaseous propellant feed system appears most promising. In general, then, the propellant supply system will consist of a vaporizer and some distribution-control system. The system currently in use for supplying alkali metal vapors to ion engines employing surface ionization systems is illustrated in figure 6.

For supplying the reactive alkali metals to our research engines, we first load the alkali metal into a small glass ampule, working in a dry nitrogen atmosphere. One or more of these ampules are then placed into the propellant vaporizer of the engine and are broken to release the propellant when desired. The vaporizer consists of a controlled-temperature container in which some liquid propellant is maintained; the pressure in the vaporizer is then the vapor pressure corresponding to the propellant liquid temperature. All other parts of the vaporizer should be kept at temperatures equal to or higher than that of the controlled-temperature basin to avoid condensation. In the device shown in figure 6 we accomplish this by jacketing the entire vaporizer and circulating thermostatically controlled oil through the jacket.

Propellant vapor issues from the vaporizer through a cluster of orifices, which are arranged to distribute the vapor in the desired pattern as it flows into the ion source. Where surface ionization is used, it is usually desired to have a uniform vapor distribution. Propellant flow rate can be varied by varying the propellant liquid temperature in the vaporizer. The flow rate through the orifices is given by:

$$\dot{m} = \frac{1}{4} \rho A \bar{v} \alpha \qquad (15)$$

where $\bar{v}$ is the average molecular velocity of random thermal motion, and α is a factor which corrects for molecular reflections occurring inside the orifice. Values from reference 3 are:

L/r	0	1	2	4	10	L≫r
α	1	0.672	0.5136	0.3589	0.1973	8r/3L

The foregoing relations are valid so long as the radius of the orifice is considerably greater than the mean free path, so that the flow through the orifices occurs by molecular effusion.

For sharp-edged orifices (L/r = 0), a cosine distribution of particles is obtained at the orifice outlet:

$$\frac{\dot{m}_\theta}{\dot{m}_{\theta=0}} = \cos \theta \qquad (16)$$

As L/r increases, the wide-angle particles undergo progressively more wall collisions inside the orifice while the zero-angle particles are unaffected (provided L is much smaller than the mean free path). Thus the outlet particle flow more closely approaches that of a paraxial beam as L/r increases. Reference 3 contains these particle distribution patterns for various L/r values. This must be considered in arranging the orifices in the distributor plate.

For ion rockets capable of supplying a high current density (several hundred amperes per square meter) the propellant vapor density in the vaporizer must be increased to supply the required flow rates and we no longer have true molecular effusion through the orifices. Experimental calibration of the orifices is then required to determine

both the flow rates and the flow efflux patterns as a function of the geometry of the system and the operating conditions. Apparatus used in this work at the NASA Lewis Research Center is shown in figure 7.

ION SOURCES

Many devices for producing ions have been built and studied for mass spectrographs, as sources for particle accelerators, etc. Many of these devices are worth considering for possible ion rocket use. In general, these devices can be categorized as follows:

E-453

(a) Surface ionization

(b) Electric arcs

(c) High-frequency electrodeless discharges

(d) Electrostatic induction of particles

(e) Oscillating-electron sources

(f) Directed electron beam sources

All six of these are under experimental investigation at Lewis. The first five appear worthy of serious consideration for electric propulsion devices (not merely for ion rockets in some cases, particularly (c)).

Surface ionization. - The alkali metals, which have the lowest ionization potentials of any family of metals, can be ionized to varying degrees by bringing them into contact with materials such as tungsten, platinum, and tungsten oxide, which have high electron work functions.

Of the various possible ion sources, the surface ionization technique shows the most promise because it is the only one that has been demonstrated to give high ionization efficiency with high-atomic-weight ions. Pioneer work on surface ionization by I. Langmuir and

Becker dates back to the 1920's, and a great deal is therefore known about the fundamentals of the process. This type ion source is receiving the greatest emphasis in the ion rocket programs at the Lewis Research Center and in several other laboratories.

Despite its prime importance in the ion rocket picture, very little will be said about the mechanism of surface ionization in this paper, because it has been so throughly covered in various publications. In addition to the early work by I. Langmuir and Becker, there are many recent publications (e.g., ref. 4), as well as an evaluation of surface ionization for ion rocket application in reference 5.

Reference 4 shows the ionization effectiveness of several metals, as follows: With tungsten, cesium is almost 100 percent ionized over a range of temperatures from 1200° to 2200° K (1700° to 3500° F). Rubidium is almost 100 percent ionized from about 1200° to 1400° K (1700° to 2060° F). For potassium, the ionization efficiency ranges from 87 percent at 1300° K (1880° F) down to 79 percent at 2400° K (3900° F). Na and Li are less than 5 percent ionized at temperatures below 2900° F. Thus, the ionization efficiency decreases with decreasing atomic weight.

On platinum surfaces the percent ionized is lower (except for sodium) than on tungsten, despite the higher electron work function of platinum. The most plausible explanation is a lower probability of isoenergetic electron transfer from the adsorbate to the metal for the case of platinum. A high probability of electron transfer may require that the electron in the ground state of the atom to be ionized have an energy that corresponds to an energy level of the conduction band of the metal (ref. 4).

At 1700° K (2600° F) sodium is 83 percent ionized on platinum.

The ratio of the number of ions evaporating from a surface to the number of atoms arriving at the surface is given by

$$\frac{N_p}{N_{a,i}} = \frac{1}{1 + \frac{\omega_a}{\omega_p} e^{\frac{-\epsilon(\Phi_e - V_i)}{kT}}} \tag{17}$$

which can be derived from the Saha-Langmuir equation. For alkali metals, the ratio of statistical weights ω_a/ω_p has a value of two, so the equation becomes

$$\frac{N_p}{N_{a,i}} = \frac{1}{1 + 2e^{\frac{-\epsilon(\Phi_e - V_i)}{kT}}} \tag{18}$$

Reference 4 indicates that equations (17) and (18) should include reflection coefficients to allow for the fact that some of the incident atoms do not come to equilibrium on the surface and, hence, do not follow the behavior indicated by the Saha-Langmuir equation. For cesium on a tungsten surface these reflection coefficients are close to zero and can be ignored.

At low surface temperatures an adsorbed layer of ions and atoms exists on the surface. The adsorbed ions serve to reduce the electron work function. Thus, in this range of temperatures, an increase in temperature increases the ion current that flows from the surface due to progressive removal of the adsorbate. With surface ionization systems for ion rockets our main concern is to stay at temperatures above this region where an adsorbed layer (and low work functions) exist. As surface temperature is increased for any fixed value of atom arrival rate

at the surface a critical temperature is reached where the adsorbed layer suddenly disappears and the ion current from the surface abruptly increases. Above this critical temperature the ion current then slowly decreases with further increase in temperature; this trend is solely due to the T influence in the exponential term of (18), since Φ_e is now substantially that of the clean metal surface. The optimum surface temperature for an ion rocket system is therefore equal to the aforementioned critical temperature. Operation at temperatures slightly above the critical values will involve only a slight performance penalty; temperatures below the critical values should be avoided unless durability considerations should make this mandatory in some cases.

The critical surface temperature depends on the arrival rate of the atoms at the surface. D. Langmuir (ref. 5) has derived empirical equation for the critical surface temperatures necessary to permit various ion current densities when the propellant feed rate is closely matched to the ion extraction rate so that no adsorbed layer exists. From Langmuir's paper, for cesium on tungsten,

$$\log_{10} i = 12.99 - \frac{14,350}{T_c} \tag{19}$$

for potassium on tungsten,

$$\log_{10} i = 10.37 - \frac{11,300}{T_c} \tag{20}$$

and for rubidium on tungsten,

$$\log_{10} i = 13.15 - \frac{15,700}{T_c} \tag{21}$$

These equations are plotted in figure 8.

We can now estimate the energy efficiency of a surface ionization system. The energy losses will be due to thermal radiation. The energy efficiency of the ion since is then defined as

$$\eta_S = \frac{P_B}{P_B + P_{RAD}} \tag{22}$$

For simple engine configurations employing surface ionization, such as those shown in figure 1, if the back side of the heated surface is shielded, $A_{RAD} = A_{ION}$. The values of η_S for this case are given in figure 9.

The solid curve in figure 9 is for the current densities that would be obtained with an accelerator length of one millimeter; one engine configuration that would permit us to obtain such a short accelerator is that shown in figure 1(b). If we assume that a one-millimeter electrode spacing is about the minimum that can be achieved in practice because of manufacturing tolerances, thermal expansion effects, etc, then the solid curve of figure 9 represents the best efficiencies obtainable with this type engine. The efficiency of the ionization system falls precipitously for values of specific impulse below about 4000 seconds. This drop in efficiency at low specific impulse is due to the very large accelerator areas that must be used due to space charge limitations on current density (eq. (5)). If the ion-emitting surface is made as large as the accelerator (fig. 1(b)), then the large area results in excessive thermal radiation losses even though the required surface temperature is somewhat lower for the low values of specific impulse (fig. 8).

The dashed curves of figure 9 show the efficiencies obtainable for different values of current density in the engine. Higher current densities mean smaller areas and smaller radiation losses. Although the required surface temperature increases with increase in current density, the required area decreases sufficiently to decrease the radiation losses.

The accelerator length increases with increase in specific impulse for any constant current density. However, for the range of specific impulse and current densities indicated in figure 9 the accelerator length are all quite short. For example, to permit an accelerator lengths of one centimeter with a current density of 200 amperes/m^2 with engine configurations like those of figure 1, we must operate at a specific impulse of 19,850 seconds.

An obvious method for increasing the permissible accelerator length and decreasing the required frontal area (hence, decreasing radiation losses) is to use a configuration like that of figure 10 where the ions are first accelerated through some large potential difference to obtain high current densities (eq. (5)) and are then slowed down to the final velocity corresponding to the optimum specific impulse. If no ions impinged on the accelerating electrode, then no energy would be expended in accelerating them to their initial high velocity. Figure 11 compares the ion source efficiencies for this type engine with those previously shown in figure 9. The dashed curves illustrate two cases: (1) the case where the ions are initially accelerated through a potential difference of 40 kilovolts (corresponding to a specific impulse of 24,500 sec) and are then decelerated to various final values of specific impulse, and (2) the case when the ions are first accelerated through a potential

difference of 1059 volts (4000 seconds) and are then decelerated. For the first case, an acceleration length of 1.31 centimeter was assumed, since the electrodes must focus the ion beam so as to avoid any appreciable impingement of the 40-kilovolt ions on the electrodes. One such electrode system is shown in figure 6. Ion impingement would produce sufficient secondary electron emission to cause a very low efficiency. For the second case, an acceleration length of one millimeter was assumed. Secondary electron emission should not be great with cesium ion energies of about one kilovolt, thus a simple, closely-spaced screen should be permissible as an accelerating electrode for this case (fig. 10).

As figure 11 shows, we can make sizeable gains in ion source efficiency at low values of specific impulse. It should be noted that these gains can be more than offset in a practical engine if any appreciable fraction of the ions strike the accelerating electrode; in which case the "accelerate-decelerate" system would be less desirable than the simple "accelerate only" system.

For values of specific impulse above about 4000 seconds the "accelerate-decelerate" system offers no appreciable increase in ion source efficiency provided that very short accelerator lengths (of the order of millimeters) can be obtained in practice with the "accelerate only" system. Such short lengths may not prove feasible, since for cesium ion velocities in excess of about 1000 ev, secondary electron emission from ion impingement on the accelerator electrode may be too severe to permit the use of simple screens as electrodes. If this

proves to be the case, then the "accelerate-decelerate" system may be necessary even for $I_{SP} > 4000$ in order to permit the lengths necessary for the use of more sophisticated electrodes.

For $I_{SP} < 4000$ the "accelerate-decelerate" system with $U_{max} = 1059$ volts shows particular promise. This system yields ion source efficiencies that are almost as high as those obtainable with higher U_{max}. Also, it may permit the use of simple screens for both the accelerating and the decelerating electrodes, since secondary electron emission is not severe for a cesium ion energy of 1059 volts (ref. 6).

If we design ion rockets for extremely high specific impulse (say, 25,000 seconds, as might be required for a trip to the outer reaches of the Solar System or even for shorter trips if substantial reductions in powerplant weight should become feasible) then the accelerate-only" system is a likely choice, since reasonable accelerator lengths are then possible with this system.

The energy efficiency η_S of a surface ionization system can be quite high for $I_{SP} > 4000$ seconds. The ionization efficiency η_i can also be very high if we can insure that each atom of propellant contacts the ionizing surface and evaporates into a region where a favorable potential gradient exists for ion extraction. For propellants such as potassium (on tungsten) or sodium (on platinum), we would like to draw off the ions after the initial contact with the ionizing surface and then have the remaining neutral atoms make another contact with the surface before escaping from the ion source. If this can be achieved

we can increase the ionization efficiency above the levels previously noted for these materials (about 87 percent, maximum, for potassium and 83 percent, maximum, for sodium).

As previously noted under PROPELLANTS, low-atomic-weight propellants such as sodium and potassium would be quite undesirable for ion rockets designed to operate at low specific impulse. The lower the propellant atomic weight, the larger the accelerator area required (since length is fixed by manufacturing considerations) and the lower the ion source efficiency. For high-specific-impulse, however, it may be desirable to use the lighter alkali-metals in preference to cesium or rubidium because of the high cost of the heavier alkali metals.

In addition to the type of surface ionization systems illustrated in figure 1, we are also investigating configurations like the one shown in figure 12.

Apparatus for more fundamental studies of surface ionization is shown in figures 13 and 14. The apparatus of figure 13 will be used to investigate various surface materials and various propellants. The apparatus of figure 14 will permit measurement of the ion current densities available from a hollow source that constitutes a reservoir of ions.

Electric arc sources. - Most of the published data on electric arc ion sources indicate low efficiencies and low current densities

for this type source. However, recent developments (largely unpublished) at several laboratories in the U. S. and abroad indicate considerable promise for such ion sources. At the Lewis Research Center we are working with the ion source shown in figure 15; this apparatus is very similar to the ion source described in reference 7. Some work with other electric arc ion sources is also planned.

High-frequency electrodeless discharges. - This type of ion source is relatively new, and it has not yet been developed into an efficient device by any of its users. We are conducting some experimental work on this technique, largely because it is such a flexible system and could be used as an ion source or plasma source, and might also be developed into an electric thermal rocket. The apparatus is shown in figure 16.

Electrostatic induction of particles. - In the strict sense, this does not constitute an ion source. However, we will arbitrarily class it as such and will refer to the multimolecule charged particles as "particle ions" (as opposed to molecular ions).

The electrostatic particle precipitator is a well-known and widely-used device. It is basically this same device that might be used to produce the particle ions. One advantage of this system may be its high efficiency. Ionization efficiencies of well over 90 percent are reported for reasonable values of energy input and precipitator size. However, the electrostatic precipitator has not been tested at the desired operating conditions for ion rockets. In industrial applications

it is normally used on gases at one atmosphere pressure with 0.5 grains, or less, of dust per cubic foot. In the ion rocket we will have zero gas feed - only solid particles. In the normal use of the device, molecular ions are formed in a corona discharge and these then pick up electrons from the dust particles to form the particle ions. At ion rocket conditions we could use much higher electric field strengths and hope to get a corona with particle ions playing the role normally played by molecular ions. Or we might use parallel, oppositely-charged plates with very high electric field strengths, and try to get conversion to particle ions through the mechanism of high-field emission of electrons from the particles. So the ionization efficiency to be expected is very much in doubt; we can only hope to attain the 90^+ percent values quoted for industrial use of electrostatic precipitators.

It may prove difficult to generate the required particles, as the requirements are rather stringent: (1) They must be quite small (of the order of 0.001 to 0.01 microns) or the required accelerating voltage becomes ridiculous. It does not appear feasible to maintain even one electronic charge on particles smaller than 0.001 microns. (2) They must consist of a very narrow range of particle sizes so that all will be ejected at close to the optimum exhaust velocity. (3) They must have a very low vapor pressure so that only a small fraction of the propellant becomes either molecular ions or uncharged vapor molecules.

The only Lewis effort on this sytem is concentrated on the problem of generating the required particles and supplying them to a precipitator to measure particle size. We will first attempt to obtain the desired particles by condensing the vapor of low-vapor-pressure materials that sublime.

ION ACCELERATORS

The method of Pierce (ref. 7) can be used to design the accelerating electrodes for a paraxial ion beam. With this method the equations

Continuity: $$i = \text{constant} = \sigma v \tag{23}$$

Conservation of energy: $$\frac{1}{2}\mu v^2 = \epsilon(\Phi_0 - \Phi) \tag{24}$$

Poisson's equation (one-dimensional): $$\frac{d^2\Phi}{dx^2} = -\frac{\sigma}{\epsilon} \tag{25}$$

E-453

are solved to determine the potential distribution along the length of the beam for maximum current density to obtain. The required electrostatic field in the charge-free region surrounding the beam is then determined from the aforementioned longitudinal potential distribution and the conditions: $\frac{d\Phi}{dr} = 0$ at the beam edge, and $\nabla^2\varphi = 0$ in the region outside the beam. The electrodes must then have the configuration of equipotential surfaces in the required electrostatic field.

Performance in accord with theory can be approached only if we restrict the accelerator to small aperture sizes and small current densities. For high current densities the accelerator length must be quite short as previously noted (eq. (5) and figs. 9 and 11). A typical Pierce accelerator is shown in figure 6. To obtain reasonable current densities it becomes necessary to (1) eliminate all but one accelerator electrode to obtain the short length required, and (2) install screens to minimize the aperture effect (bowing of the potential ines through the aperture in the accelerating electrode). With screens installed in the electrode aperture, secondary electron emission from the screen will probably set the upper limit on the accelerating voltage (hence, current density).

Another design approach is obtained using strip beams (long narrow beams) in order to keep the aperture effect to a minimum. The design techniques employed in high-perveance electron guns can be used to advantage here. A strip-beam ion engine employing an accelerator designed after the method of Brewer (ref. 8) is shown in figure 17. The electrostatic field approaches the theoretical field existing between concentric cylinders (for example, ref. 9). The voltage and position of the focussing electrodes are variable to compensate for aperture and space charge effects.

An interesting configuration suggested by David Lockwood of the Lewis Research Center is shown in figure 18. The principles are the same as in the engine of figure 17 except that the ion flow is now from the inner cylinder through the aperture in the outer cylinder. This configuration permits us to take advantage of the high potential gradients that exist at the inner cylinder; thus, with no ion flow, we have the highest potential gradients in the region where space charge effects will be most severe.

With strip-beam ion accelerators, a practical ion engine will obviously consist of some closely-packed array of these devices.

We can define an ion accelerator efficiency as

$$\eta_A = \frac{P_B}{P_B + P_A} \tag{26}$$

for a simple case where a single accelerator electrode is used. P_A is the power input to the accelerator electrode. Electron emission from the accelerator electrode will have the same effect on efficiency as ion impingement, assuming that the electrons "fall" back to the ion source.

Then

$$\eta_A = \frac{I_B}{I_B + I_A} \tag{27}$$

where I_A is the current drawn by the accelerator electrode. Some data (e.g., ref. 10) indicate that values of η_A above 90 percent can be obtained.

ELECTRON EMITTERS

If we suddenly turned off the flow of electrons that are injected into the ion beam as it leaves the ground electrode of the accelerator and if the beam were one-dimensional (no divergence), then the ions would come to a standstill after travelling a distance L (equal to the accelerator length) downstream of the ground electrode. Beam current and thrust then drop to zero. In other words, equation (5) also applies outside the engine. If we are to approach the full current-density capability of the ion accelerator, we must therefore achieve neutralization of the exit space charge in a very short distance.

Space charge effects dictate a low particle density at the exit end of the ion rocket. For a 1.31 cm accelerator length and U = 40,000 volts, we will have an exit particle density of $5.7\times10^{15}/m^3$. At this static pressure $p = \frac{n}{n_{NTP}} = \frac{5.7\times10^{15}}{2.69\times10^{25}} = 2\times10^{-10}$ the half-life of a completely ionized plasma will be of the order 10^5 sec, assuming radiative recombinations to be predominant. Hence, a negligible fraction of the ions and electrons will recombine before striking the wall of our test chambers.

Space-charge neutralization can nevertheless be effected in a very short distance (in theory) if we can inject the electrons at approximately the same

velocity as the ions and can disperse the electron source throughout the ion beam. The simplest and most obvious way of doing this would be to place an electron-emitting grid across the outlet of the ion accelerator as in figure 17 or to place the emitting wires about the periphery of the ion beam. Another obvious technique is to use electron guns at the exit of the ion accelerator. Electron guns permit control of the initial electron beam direction and can also provide some control of initial electron velocity, particularly if some accelerate-decelerate system is employed in the electron gun. Regardless of which system is used to introduce the electrons, some interesting problems arise.

Analysis of a one-dimensional beam, carried out by H. R. Kaufman of the Lewis Research Center, indicates that a steady-state beam is impossible unless $v_e < 2v_i$ for the case where the ions and electrons are interspersed but have different initial velocities. For $v_e > v_i$ but $v_e < 2v_i$ the electrons undergo a longitudinal oscillation at the plasma frequency; this oscillation is superimposed on their through-flow velocity. The oscillation is triggered by the fact that $\rho_i > \rho_e$ in the region where $v_e > v_i$, thus leaving a positive space charge in that region which slows down the electrons until $v_e < v_i$ and $\rho_e > \rho_i$ in the next half-wave-length segment of the beam.

Let us examine the possibility of using electron guns to give $v_e < 2v_i$. If we assume that initial (thermal) electron velocities are negligible, then for $I_i = I_e$, from equation (5),

$$\frac{A_e}{A_i} = \left(\frac{\mu_e}{\mu_i}\right)^{1/2}\left(\frac{U_i}{U_e}\right)^{3/2}\left(\frac{L_e}{L_i}\right)^2 \qquad (28)$$

and from (6),

$$\frac{v_e}{v_i} = \left(\frac{\mu_i}{\mu_e}\right)^{1/3}\left(\frac{L_e}{L_i}\right)^{2/3}\left(\frac{A_i}{A_e}\right)^{1/3} \tag{29}$$

Now take the most favorable case of an "accelerate-only" ion rocket designed for very high specific impulse (e.g., 20,000 seconds) so that we have an ion accelerator length in the neighborhood of one centimeter; L_e/L_i can perhaps be made as low as 0.1. So, for $L_e/L_i = 0.1$ and for C_s^+ ions ($\mu_i/\mu_e = 244{,}000$), these equations become:

$$\frac{A_e}{A_i} = 2.03\times10^{-5}\left(\frac{U_i}{U_e}\right)^{3/2} \tag{30}$$

and

$$\frac{v_e}{v_i} = 13.5\left(\frac{A_i}{A_e}\right)^{1/3} \tag{31}$$

A plot of these equations is shown in figure 19. It is obvious that the electron velocity at the outlet of the engine cannot be reduced to desired values without making the electron guns many times as large as the ion accelerator (again, assuming that L_e/L_i has a lower limit of about 0.1).

Our salvation may lie in the departure from a one-dimensional ion beam. We do not have an infinite ion beam, so beam divergence may help somewhat. But our big hope lies in the extreme mobility of the electrons and their tendency to be drawn radially inward into the core of the ion beam. We can tilt the electron guns to vary the initial electron beam direction. The optimum initial angle can be determined by experiment. The final result may be something like the sketch in figure 20(a). As $v_{e,x}$ approaches v_i we should get over-all neutrality in the beam.

To achieve the required space charge neutralization without having electrons "fall" back into the ion accelerator may necessitate the use of a decelerating field at the end of the ion accelerator.

At best, it appears that a certain amount of power will be wasted as the positive ions move into a positive-space-charge region at the engine exit. In a practical configuration, the ions will not "fall" through a zero-potential plane and attain their ideal exhaust velocity even though the final accelerating electrode is kept at ground potential. The potential field at the exit may be such that some (or all) of the ions decelerate after leaving the final electrode. In this case the final ion velocity (at the point where beam neutralization finally occurs) is the one of interest. The positive space charge region aft of the engine will exert a drag and will counterbalance the internal (thrust) force obtained by accelerating the ions above their final velocity.

As indicated in figure 20(b), we may be able to reduce the power loss that would otherwise accrue from the above phenomenon, by operating the final ion accelerating electrode at a lower potential than the electron guns. In theory, the electron emitter need be at only a few volts lower potential than that of the positive ion space charge region into which the electrons are to flow. In which case, the input power used in pumping the electrons from the high-potential ionization grids to the potential of the emitter, or electron-gun cathode, is still substantially the same as the ion beam power. The only net loss through such a procedure would then be a lower value of η_A than if $U_{actual} = U_{theoretical}$.

Some finite time is required for the electrons to flow into the ion beam, and the ions continue to decelerate and build up a higher space charge during this time. Consequently, we may be forced to inject the electrons upstream of the point of highest potential in the exit space charge region. Then, the actual ion beam power $P_{B,A}$ will be less than

the electrical input power required in pumping electrons $P_e \approx P_B$. Hence, we define another efficiency term

$$\eta_E = \frac{P_{B,A}}{P_e} = \frac{P_{B,A}}{P_B} \tag{32}$$

OVER-ALL EFFICIENCY

From our preceding definitions of component efficiencies (η_i, η_s, η_A, and η_E) we can define an over-all ion rocket efficiency η_R as follows:

$$\eta_R = \frac{P_{B,A}}{P_{in}} \eta_i = \frac{P_B}{P_{in}} \eta_i \eta_E$$

$$= \eta_i \eta_E \left(\frac{1}{\frac{1}{\eta_S} + \frac{1}{\eta_A} - 1} \right) \tag{33}$$

The individual component efficiencies have been defined in such a way that the values for each component reflect the true influence of that component on the over-all engine efficiency; that is, the specified value for the particular component under consideration is equal to the over-all efficiency if all other component efficiencies are 100 percent.

Some speculation as to the attainable values of over-all efficiency seems in order at this point. For a surface ionization system η_i can closely approach 100 percent and η_S will have the calculated values of figures 9 and 11. The values of η_A must be determined experimentally for any accelerator of interest; values in excess of 90 percent may be feasible. The biggest unknown quantity in equation (33) is the value of η_E; no general agreement currently exists as to its probable magnitude.

If we assume $\eta_i = 1.00$, $\eta_A = 0.90$, $\eta_E = 0.95$, and read η_S from figure 9 for a current density of 200 amperes/m^2 and a specific impulse of 10,000 seconds, we compute an over-all efficiency, $\eta_R = 84$ percent.

For low values of specific impulse the over-all efficiency will decrease, primarily because of the decreased energy efficiency of the ion source.

ENGINE TEST FACILITIES

General Requirements

Large vacuum tanks are required to permit tests of small-scale ion rockets with ample space for installing the necessary instrumentation to study beam spreading rates and exit space charge effects. Several such tanks have been designed and the first of these was recently installed at the Lewis Research Center. It is shown in figure 21, and the refrigerated condenser baffles which are installed inside the tank are shown in figure 22. Without the condenser baffles more than fifty 32-inch oil diffusion pumps would have been required to obtain a pressure of even 10^{-6} mm mercury inside the tank with a one-ampere ion beam entering the tank. With the condenser baffles, however, we expect to operate at pressures below 10^{-7} mm using only two 32-inch oil diffusion pumps. The tank diameter is 5 feet; it is 16 feet, 8.75 inches long; the condenser baffles have 730 square feet of area and can be cooled with either water or liquid nitrogen. Ample facilities for storing and transporting liquid nitrogen are already available at Lewis, thus making liquid nitrogen particularly convenient for use in the tank.

Pressures below 10^{-7} mm mercury were desired to minimize gas focussing of the ion beam. If the tank pressures are much above 10^{-7} mm, collisions between the high-velocity ions and neutral molecules will result in considerable secondary ions and electrons. If the beam is positively charged, the low energy secondary ions will be forced away

from the beam and the secondary electrons will be drawn into the beam to help in neutralizing it. The secondary electrons thus affect the external space charge and this, in turn, can affect internal engine performance. Low tank pressures were therefore deemed essential for any realistic experimental evaluation of engine performance

Theoretical Considerations

Theoretical considerations pertinent to the design of our ultra-high vacuum condenser system have been published in reference 11. The equation for the required condenser surface area is

$$S = \frac{N\mu v_0}{2p}\left[1 + (1 - f)(1 - a)^{1/2}\right](1 - f)(1 - a)^{1/2} \qquad (34)$$

It was derived for the case where the pressure is constant throughout the array of condenser baffles and the accommodation and sticking coefficients (a and f) are also constant throughout the tank. Actual conditions inside the tank may depart considerably from these assumptions, and tests currently underway are aimed at evaluating the assumptions.

Figure 23 presents the parameter $2pS/N\mu v_0$ as a function of the sticking and accommodation coefficients. For the design conditions of our first vacuum tank: $S = 730$ ft^2 (67.8 m^2); $N\mu = 1.38\times10^{-6}$ kg/sec for a one-ampere beam of cesium ions; and v_0 has a maximum value of 5.36×10^4 m/sec, assuming an accommodation coefficient of 0.95 for the initial impact of the beam on the water-cooled target inside the tank. For these conditions various tank pressures are also indicated on figure 23.

Experimental Performance

Figure 24 shows the pressure-time history for a typical test where the vacuum system was operated with no engine inside the tank. The elapsed time is measured from the time at which the oil-diffusion pumps were started. The pressures are the average readings of ionization gages located at both ends of the tank. The two discontinuities in the curve are the result of adding liquid nitrogen to the pump-inlet baffles and to the main condenser baffles, as noted on the figure.

A pressure of 7×10^{-8} mm mercury was reached after about 16 hours of operation of the oil-diffusion pumps. Approximately this same pressure is obtained in most tests where the system is free from leaks before beginning the test. In one test in which the main condenser baffles were removed from the tank, a pressure of 2×10^{-8} mm mercury was obtained.

The combined leakage and outgassing rate, as determined from the measured rate of pressure rise with the pumps off, ranges between 4×10^{-3} and 6×10^{-3} mm mercury per hour with the main condenser baffles installed but with the metal surfaces at room temperature. The leakage plus outgassing rate is about 1×10^{-3} mm mercury per hour with the baffles filled with liquid nitrogen.

Two tests have been conducted in which sodium vapor was added to the tank. The data are shown in the following table:

Sodium flow rate $N\mu$ (kg/sec)	Pressure before sodium addition (mm Hg)	Pressure during sodium addition (mm Hg)	$\frac{2Sp}{N\mu v_0}$ during sodium addition	Possible values of a and f
6.39×10^{-7}	5.7×10^{-6}	5.7×10^{-6}	37.8	
3.61×10^{-5}	1.1×10^{-7}	6×10^{-7}	5.64×10^{-2}	$f = 0.765$ if $a = 0.95$

The first test involved such small sodium flow rates that no pressure rise would be expected, and none was observed. This test was conducted primarily to evaluate the procedures for removal of alkali metal from the condenser baffles. This procedure is quite simple: The tank pressure is slowly increased to atmospheric pressure by admitting carbon dioxide into the tank. This presumably converts the alkali metal to the carbonate. The tank is then opened and the condenser baffles are removed and washed with water. There has been no indication of any chemical reaction during this procedure, thus indicating that the conversion to the carbonate is substantially complete. Earlier tests in a bell jar apparatus with chemical analysis of the condensed material had also indicated complete conversion to the carbonate.

The second test served to indicate the effective over-all values for the sticking and accommodation coefficients. Of course, various combinations of values for a and f would account for the observed result, as indicated in figure 23. But if we arbitrarily assume $a = 0.95$, than $f = 0.765$, as indicated in the table. If the same values of a and f apply for actual ion rocket operation with considerably higher v_0 but much lower mass flow rates, then a pressure of about 2×10^{-6} mm

mercury is about the lowest that we might expect to maintain in the condenser section of the tank for steady-state operation with a one-ampere ion beam.

During operation of an actual ion rocket, however, the ion beam will serve as an ejector and may reduce the pressure forward of the bulkhead (see fig. 21(b)) to a value substantially below the pressure existing in the condenser section of the tank. If this occurs, then we might obtain quite low pressures near the engine. If a neutral plasma can be obtained before the beam passes through the opening in the bulkhead, we might then be relatively free of gas-focusing effects. If the beam is not electrically neutral, however, a back-flow of electrons from the condenser section of the tank could occur.

APPENDIX - SYMBOLS

A	area (m^2)
a	accommodation coefficient
E	electric field (volts/m)
ϵ_0	permittivity of free space (8.854×10^{-12} farads/m)
F	thrust (kg)
f	sticking coefficient
g	gravitational acceleration (9.81 m/sec^2)
I_B	ion beam current, amperes
I_{SP}	specific impulse, sec
i	current density ($amperes/m^2$)
i_s	saturation current density ($amperes/m^2$)
k	Boltzmann constant
L	length (m)
m	mass (kg)
$\dot{m}$	mass flow rate (kg/sec)
N	particle flow rate $(sec)^{-1}$
n	number of particles per cubic meter
P	power (KW)
p	pressure kg/m^2 in equations; mm Hg in tabulations
r	radius (m)
S	surface area (m^2)
T_c	critical temperature in the surface ionization process, ^oK
U	total potential difference across electrostatic accelerator (volts)

V_i ionization potential, volts

v velocity (m/sec)

ϵ ion charge (1.602×10^{-19} coulomb for singly-charged ion)

η_A accelerator efficiency; $\eta_A = \dfrac{P_B}{P_B + P_A} \approx \dfrac{I_B}{I_B + I_A}$

η_E exit-space-charge efficiency factor; $\eta_E = \dfrac{P_{B,A}}{P_e} \approx \dfrac{P_{B,A}}{P_B}$

η_i ionization efficiency, mass ratio of ions to total material leaving ion source

η_R over-all ion rocket efficiency; $\eta_R = \eta_i \eta_E \left(\dfrac{1}{\frac{1}{\eta_S} + \frac{1}{\eta_A} - 1} \right)$

η_S energy efficiency of ion source; $\eta_S = \dfrac{P_B}{P_B + P_{RAD}}$

μ particle mass (kg)

μ_e electron mass (9.108×10^{-31} kg)

ρ density (kg/m^3)

σ charge density ($coulombs/m^3$)

φ potential (volts)

Φ_e electron work function (volts)

ω_a/ω_p ratio of statistical weights ($\omega_a/\omega_p = 2$ for alkali metals)

Subscripts:

a neutral atoms

a,i incident neutral atoms

A accelerator or accelerator electrode

B beam (ideal)

e electrons

i, p	ions
0	condition of particles inside test facility after rebounding from target
in	electric input
NTP	normal temperature and pressure
RAD	thermal radiation

REFERENCES

1. Moeckel, W. E.: Propulsion Methods in Astronautics. Paper presented at Int. Cong. Aero. Sci., Madrid (Spain), Sept. 13, 1958.

2. Child, C. D.: Phys. Rev., 32 (1911) 492.

3. Dayton, B. B.: Gas Flow Patterns at Entrance and Exit of Cylindrical Tubes. Consolidated Electrodynamics Corp., Sept. 13, 1956.

4. Datz, Sheldon, and Taylor, E. N.: Jour. Chem. Phys., 25, 389 (1956).

5. Langmuir, D. B.: Problems of Thrust Production by Electrostatic Field. Paper presented at AFOSR Astronautics Symposium, Revier (Colo.), Apr. 28-30, 1958.

6. Massey, H. S. W., and Burhop, E. H. S.: Electronic and Ionic Impact Phenomena. Clarendon Press (1956).

7. Pierce, J. R.: "Theory and Design of Electron Beams." D. Van Nostrand Co., Inc., (1954).

8. Brewer, George R.: Formation of High-Density Electron Beams. Jour. Appl. Phys., 28, 7-15 (1957).

9. Marten, L.: Advances in Electronics and Physics, Vol. VI. Academic Press, (1954), p. 239.

10. Anderson, Carl E.: "Ion Source for the Production of Multiply Charged Heavy Ions." Rev. Sci. Inst., 27 (1956) pp. 809-817.

11. Mickelsen, William R., and Childs, J. Howard: Theoretical Analysis of Ultrahigh Vacuum Condensers. Rev. Sci. Inst., 29, 871-873 (1958).

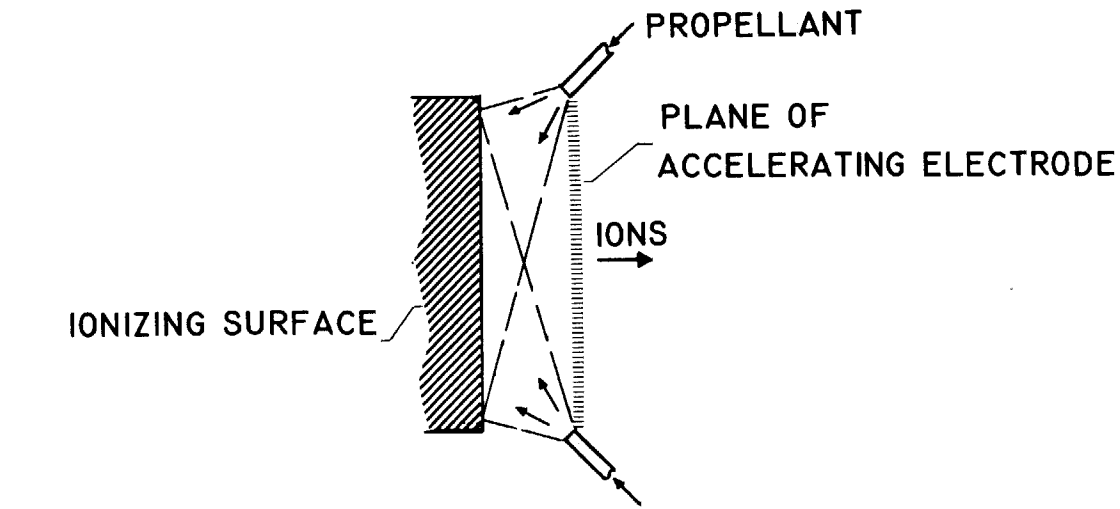

(A) CONFIGURATION WITH REVERSED FLOW PROPELLANT FEED

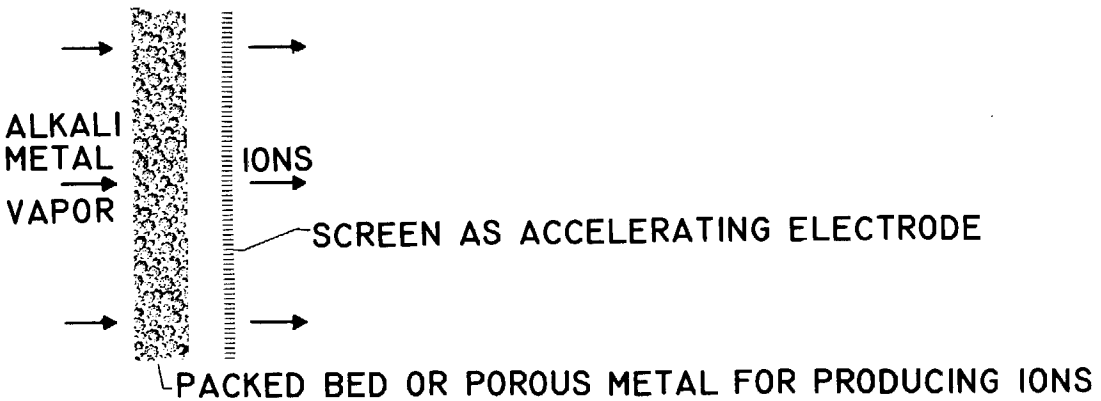

(B) CONFIGURATION WITH CLOSELY-SPACED SCREEN AS ACCELERATING ELECTRODE

Figure 1. - Two simple ion rocket configurations.

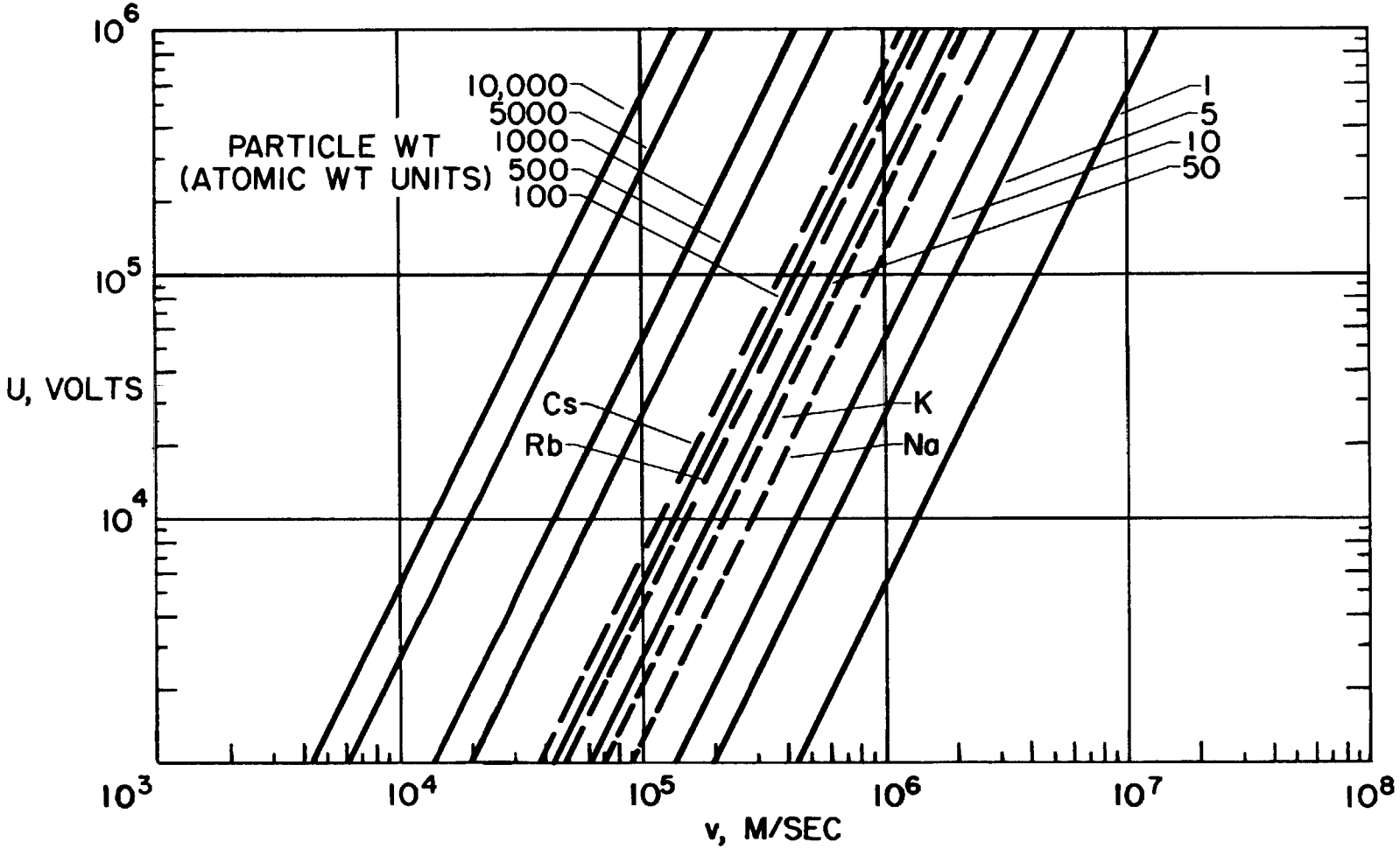

Figure 2. - Ion velocities.

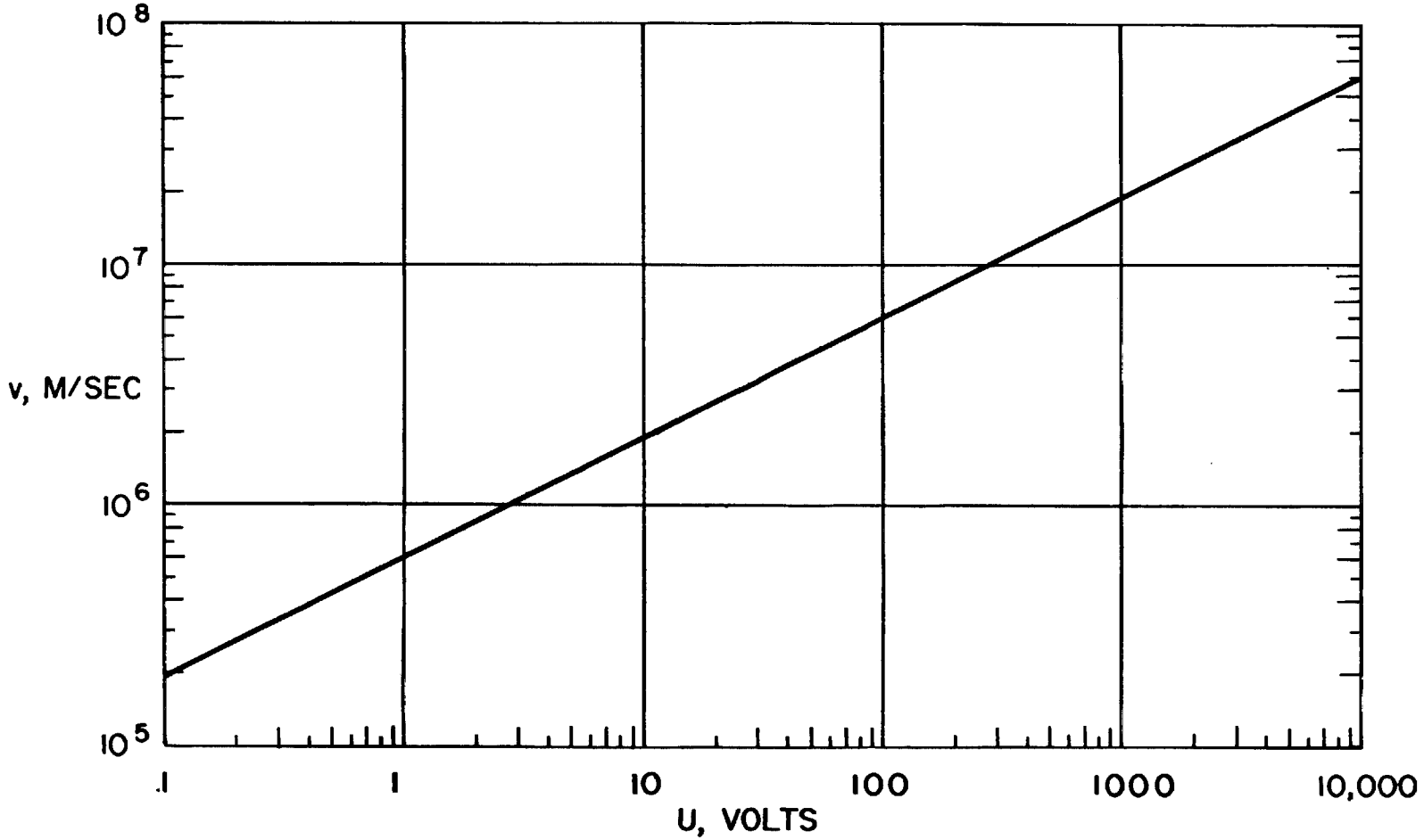

Figure 3. - Electron velocities.

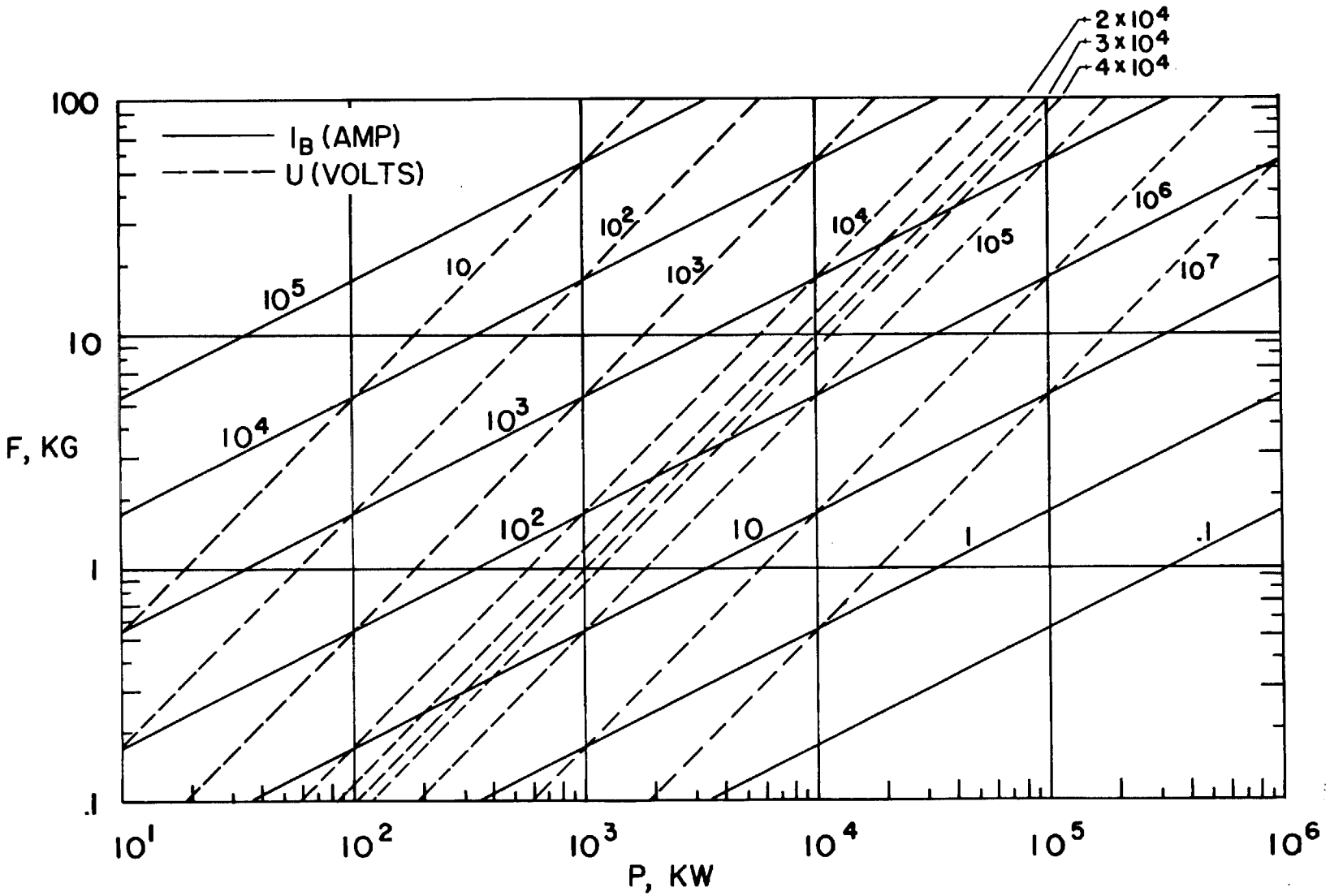

Figure 4. - Ion rocket power and thrust. Cesium ions.

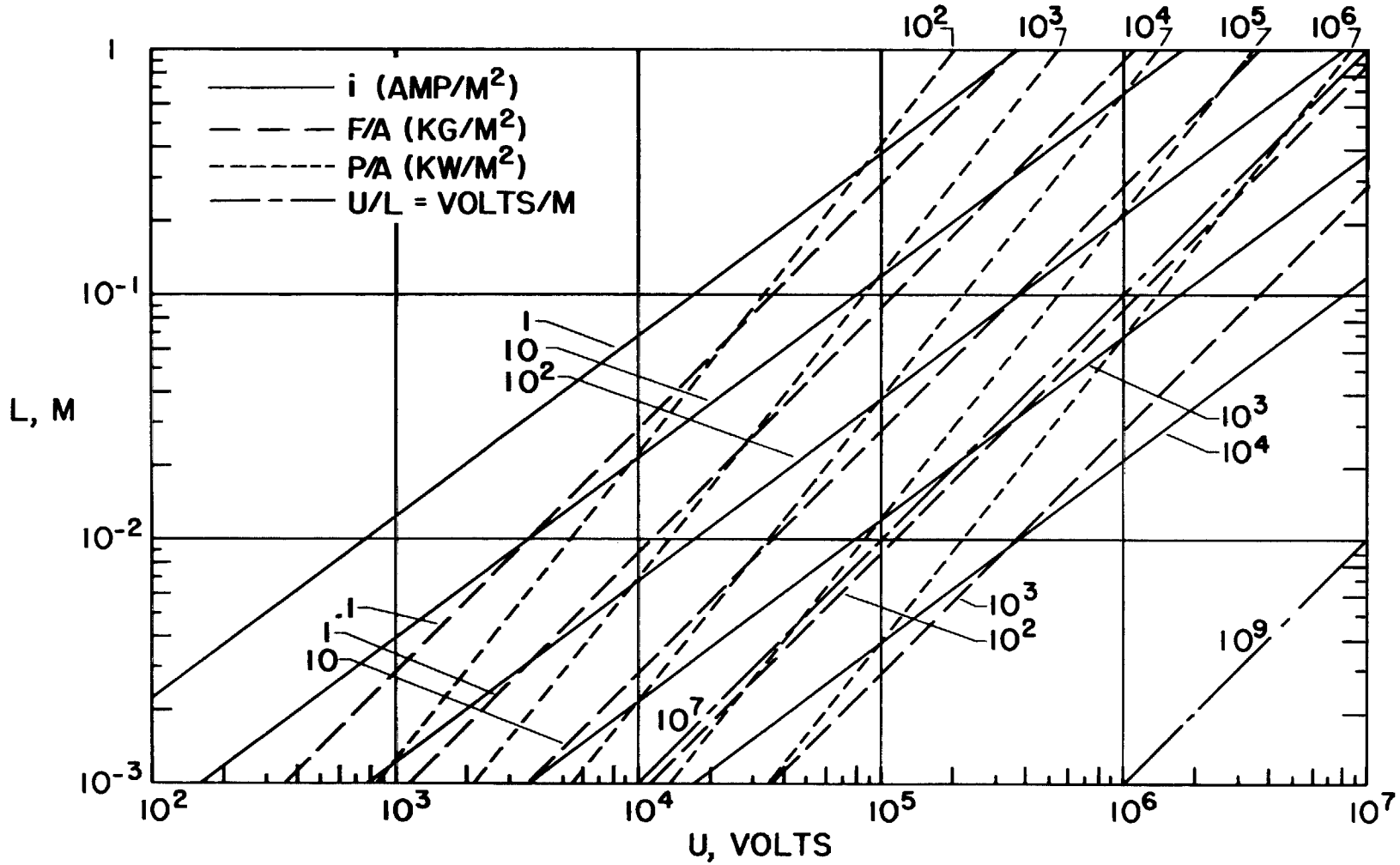

Figure 5. - Effect of over-all design on ion rocket output per unit area. Cesium ions.

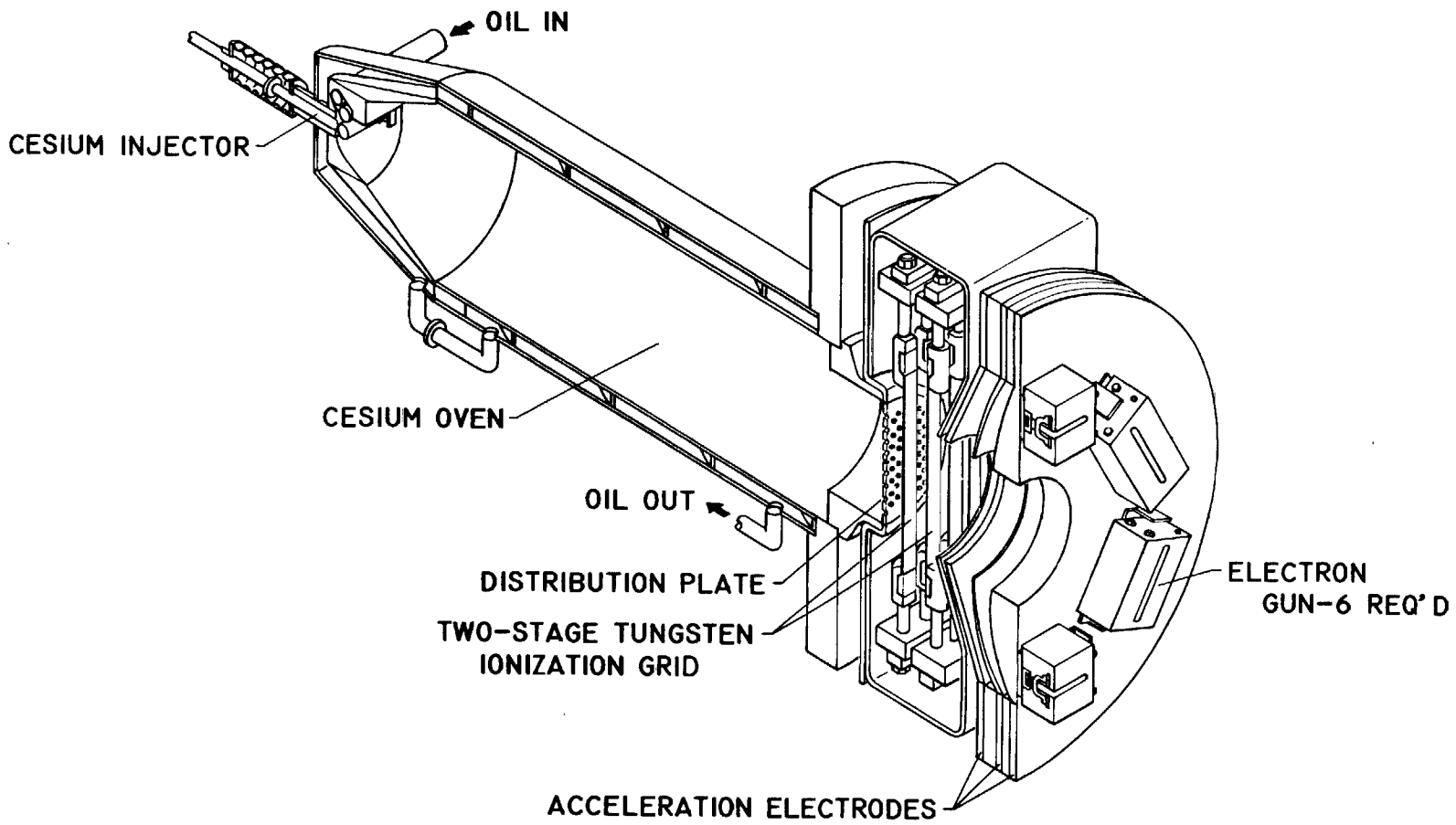

Figure 6. - Ion rocket employing paraxial Pierce electrodes with variable configuration.

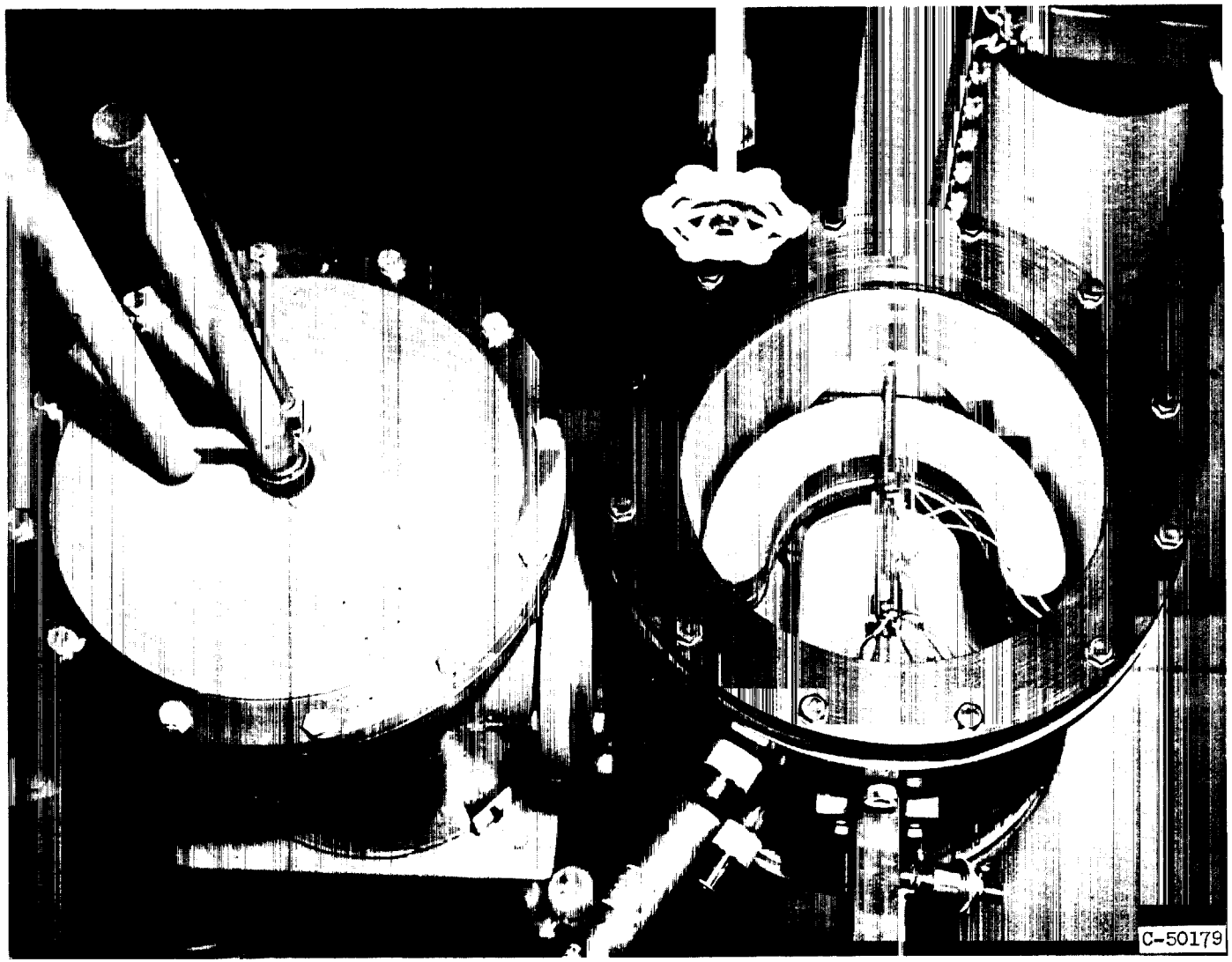

(a) Photograph of apparatus.

Figure 7. - Apparatus for measuring propellant flow rates and efflux patterns.

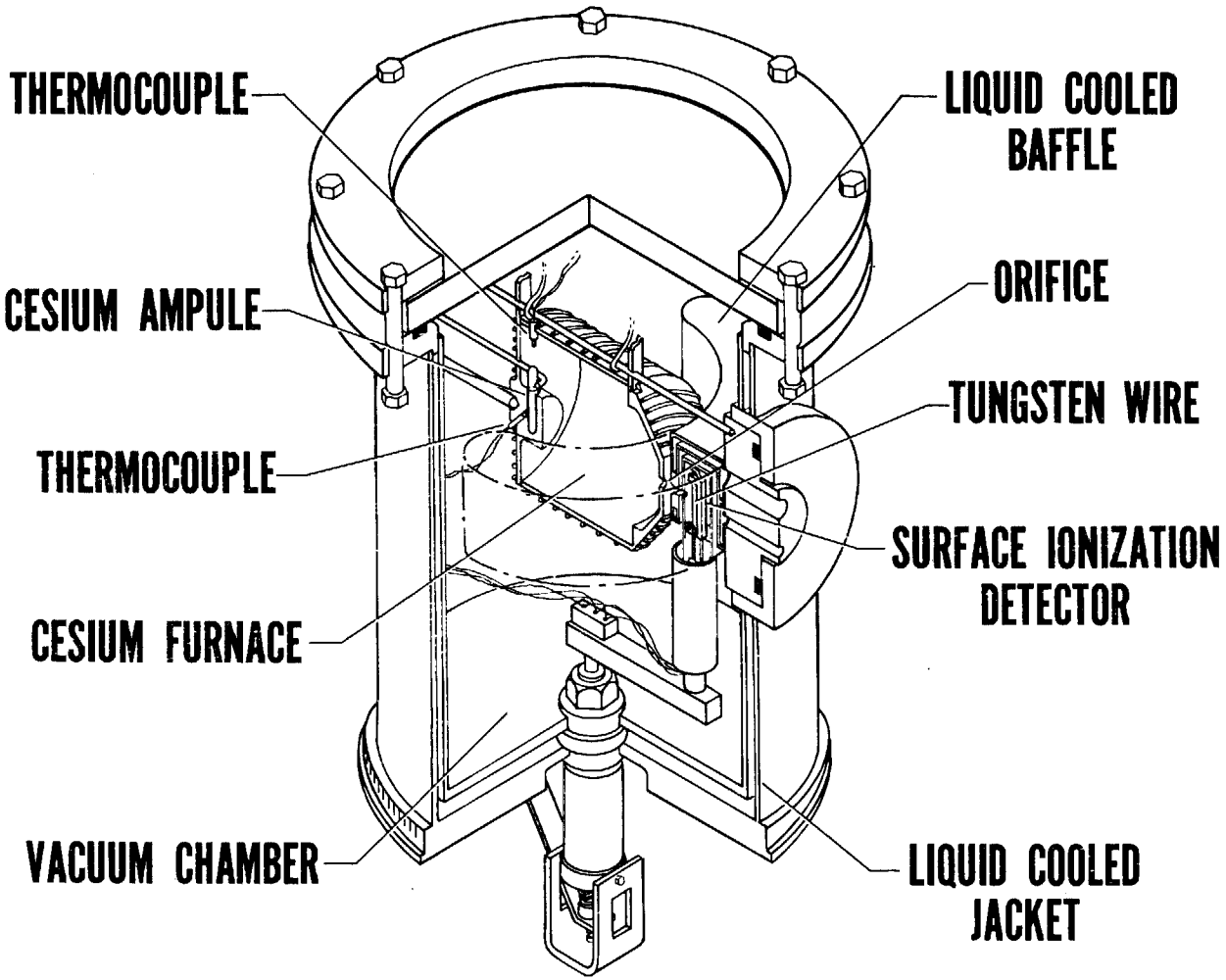

(b) Diagram of apparatus.

Figure 7. - Concluded. Apparatus for measuring propellant flow rates and efflux patterns.

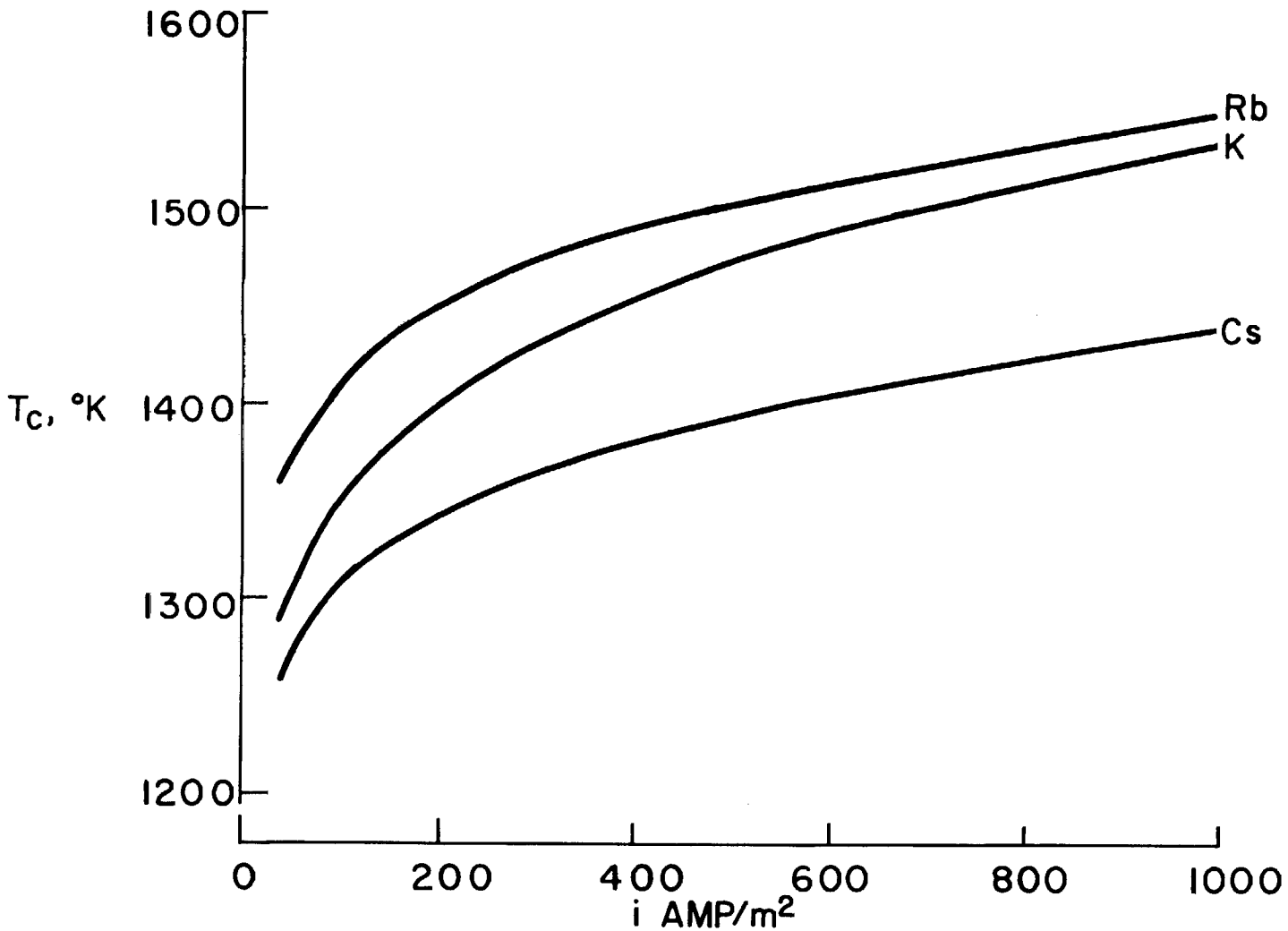

Figure 8. - Critical temperatures for surface ionization on tungsten (from ref. 5).

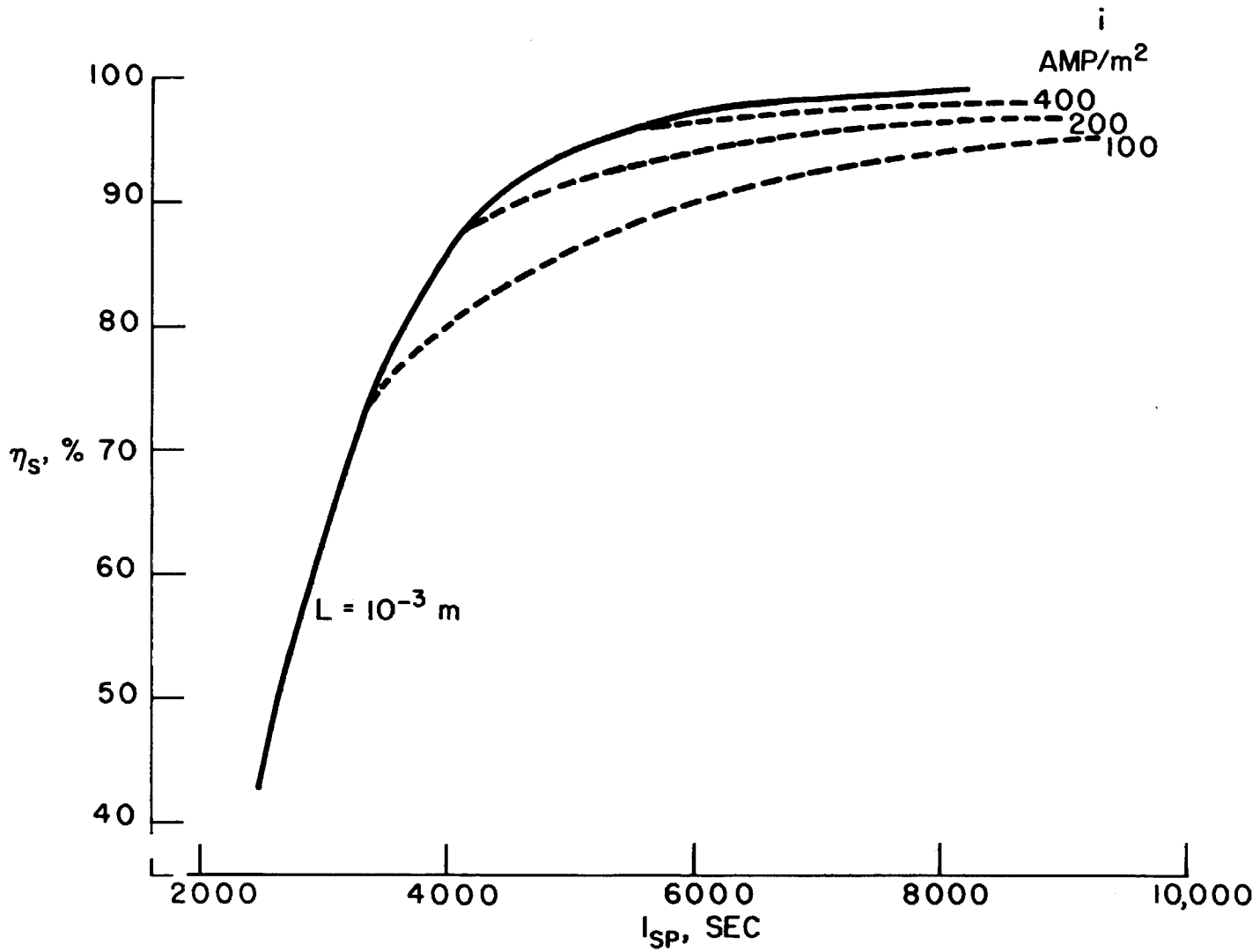

Figure 9. - Energy efficiency of ion rocket surface ionization system. Tungsten surface. Cesium propellant.

E-453

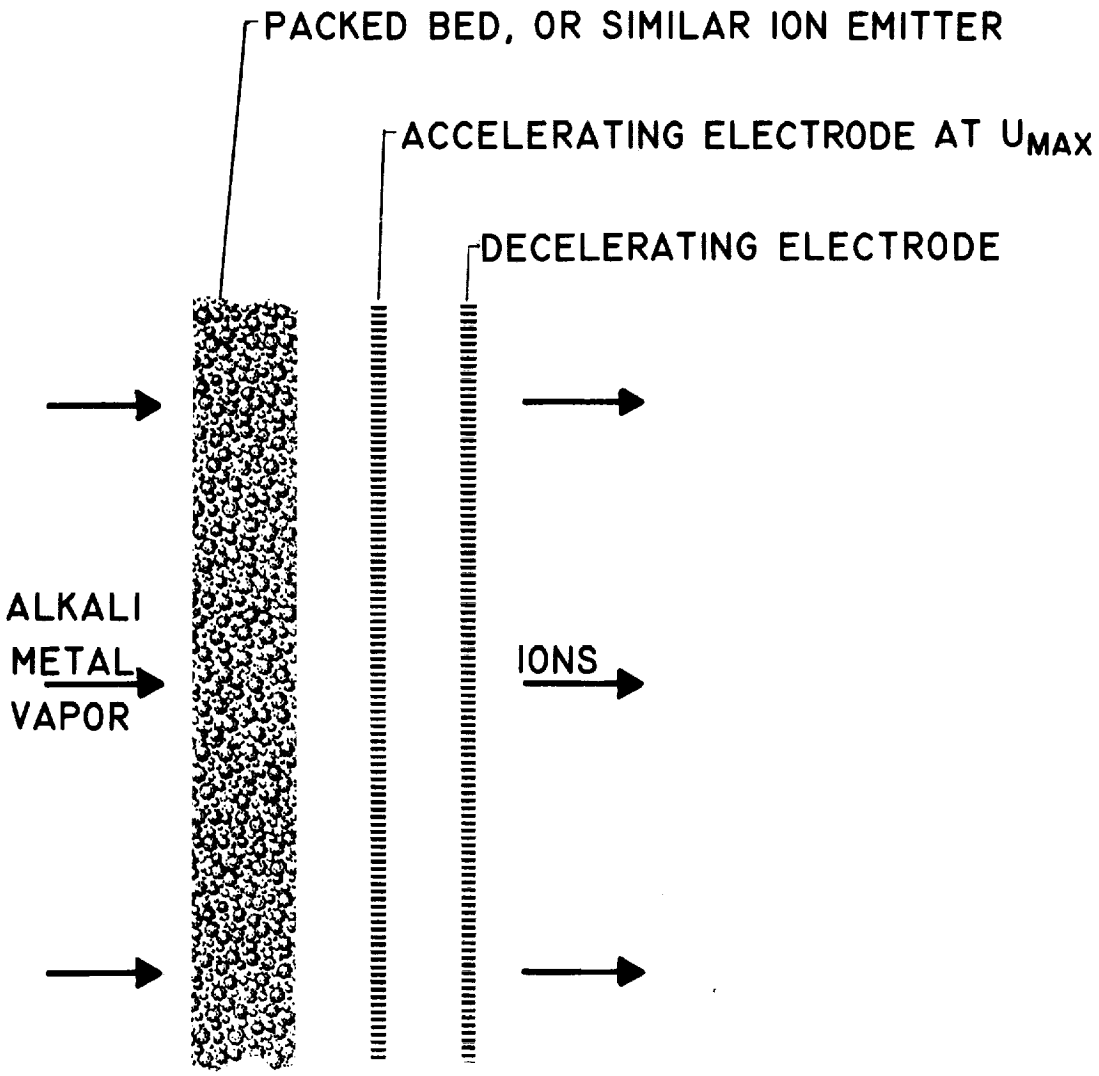

Figure 10. - A simple ion rocket employing the "accelerate-decelerate" principle.

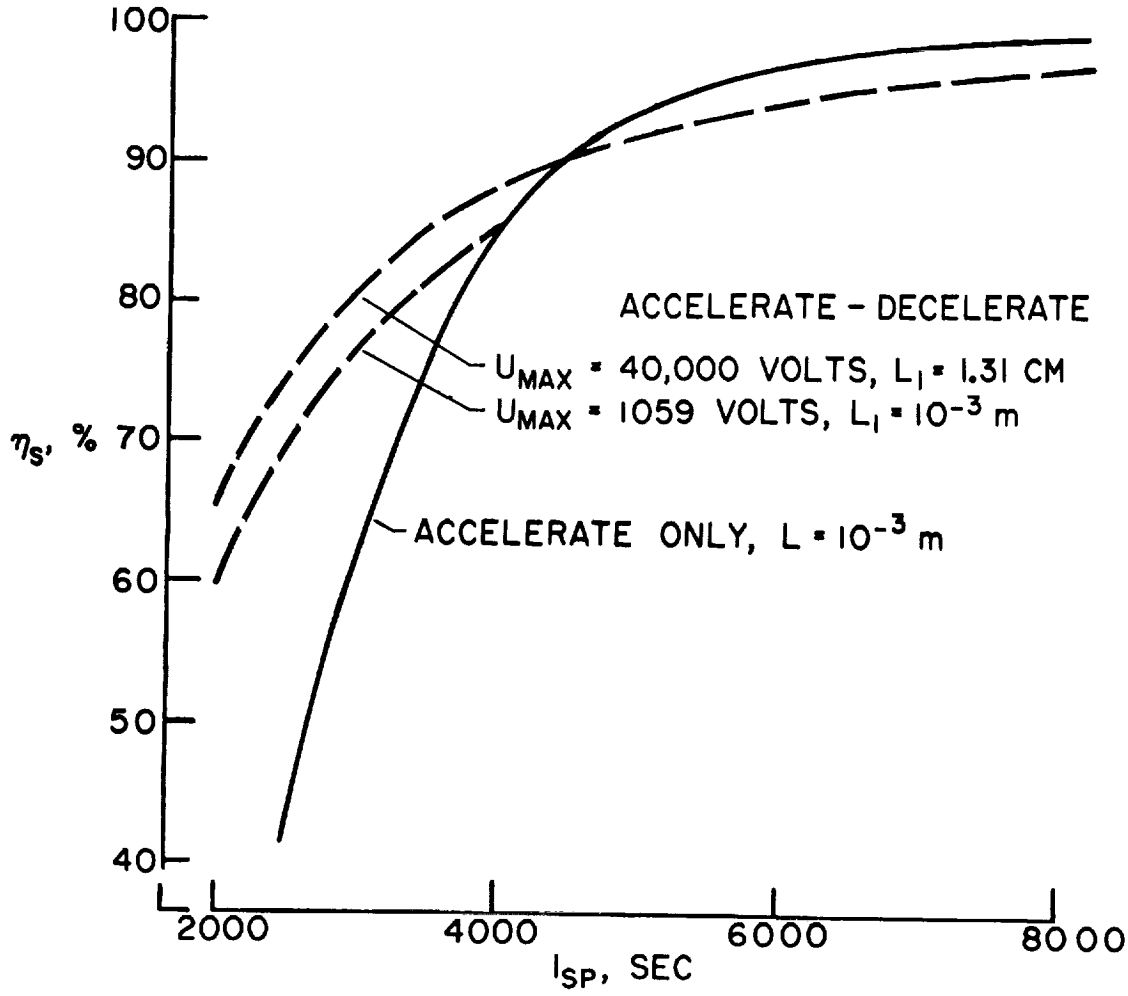

Figure 11. - Energy efficiency of ion rocket surface ionization system for cases where a high voltage is used to pull high current densities from the system. Tungsten surface. Cesium propellant.

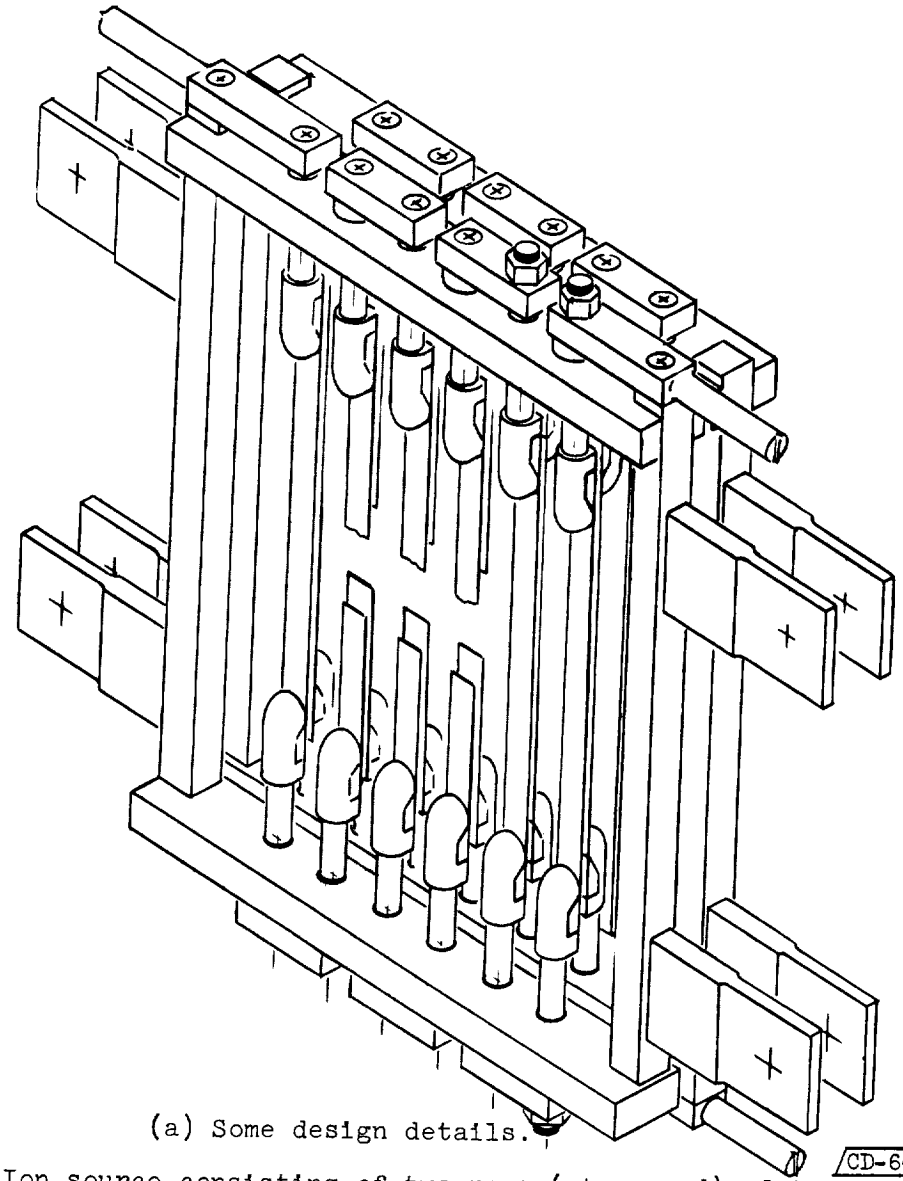

(a) Some design details.

CD-6469

Figure 12. - Ion source consisting of two rows (staggered) of tungsten strips individually supported in tension and electrically heated by a current passing in series through the strips.

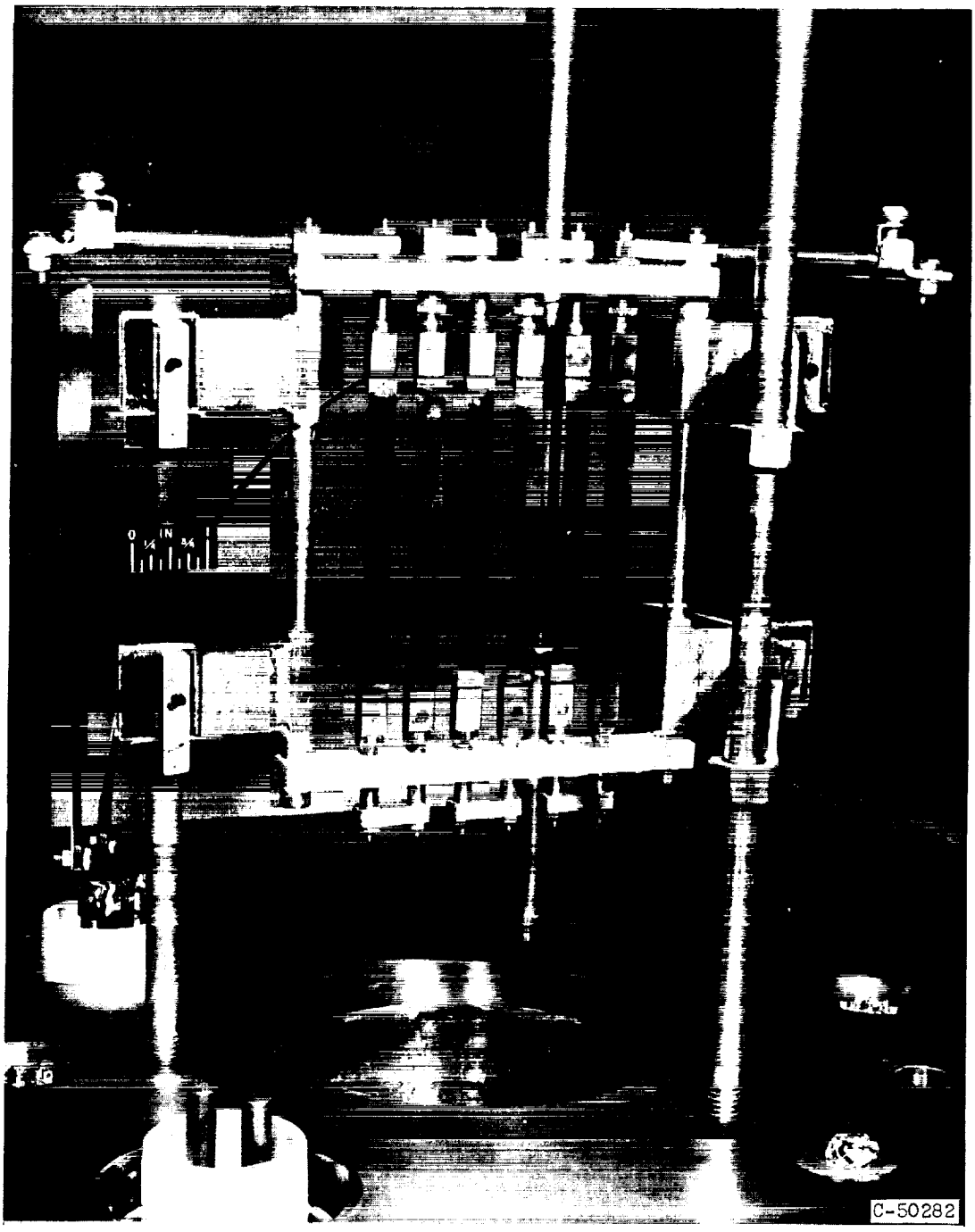

(b) Photograph of a single tungsten grid.

Figure 12. - Concluded. Ion source consisting of two rows (staggered) of tungsten strips individually supported in tension and electrically heated by a current passing in series through the strips.

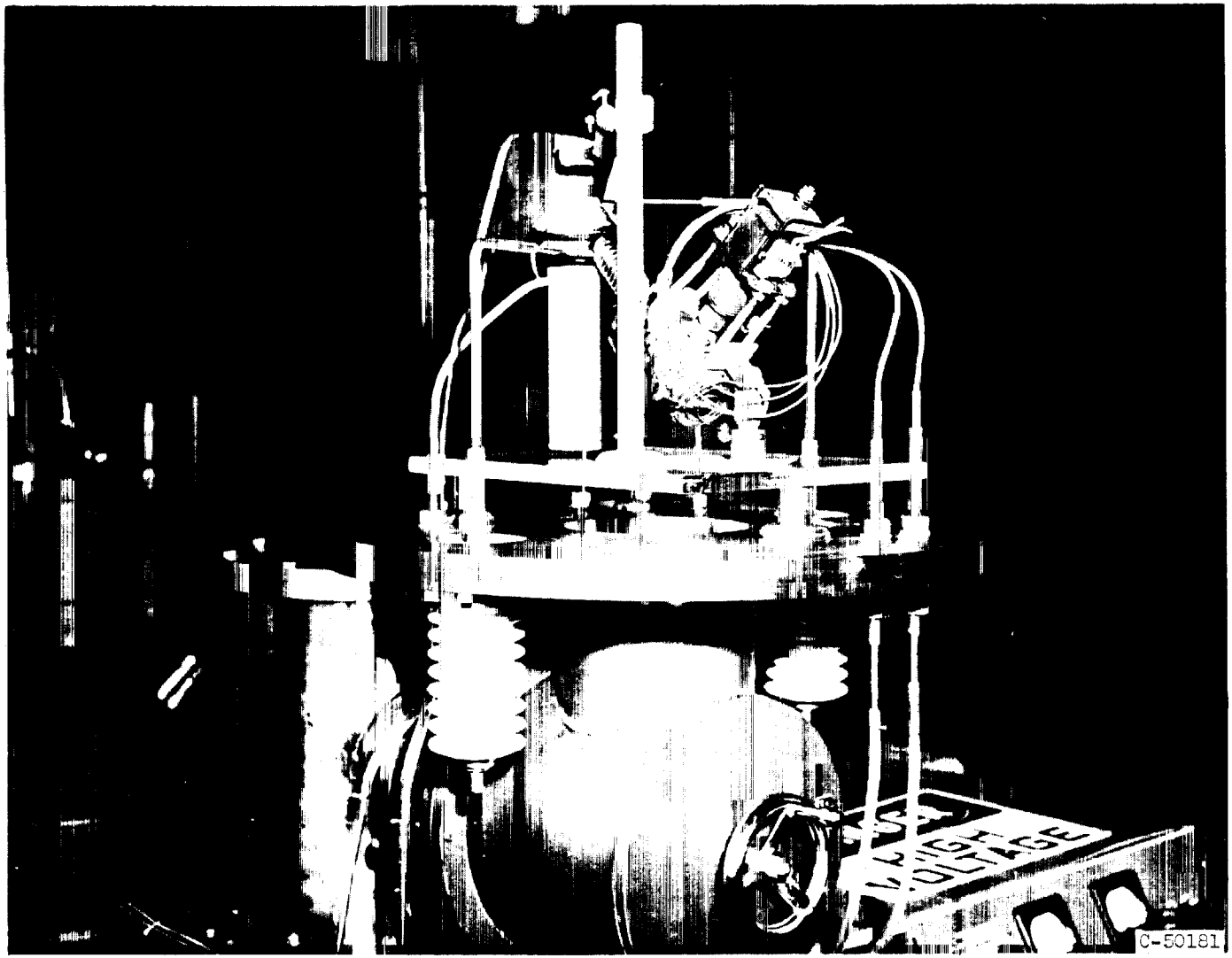

(a) Photograph of apparatus.

Figure 13. - Apparatus for surface ionization studies.

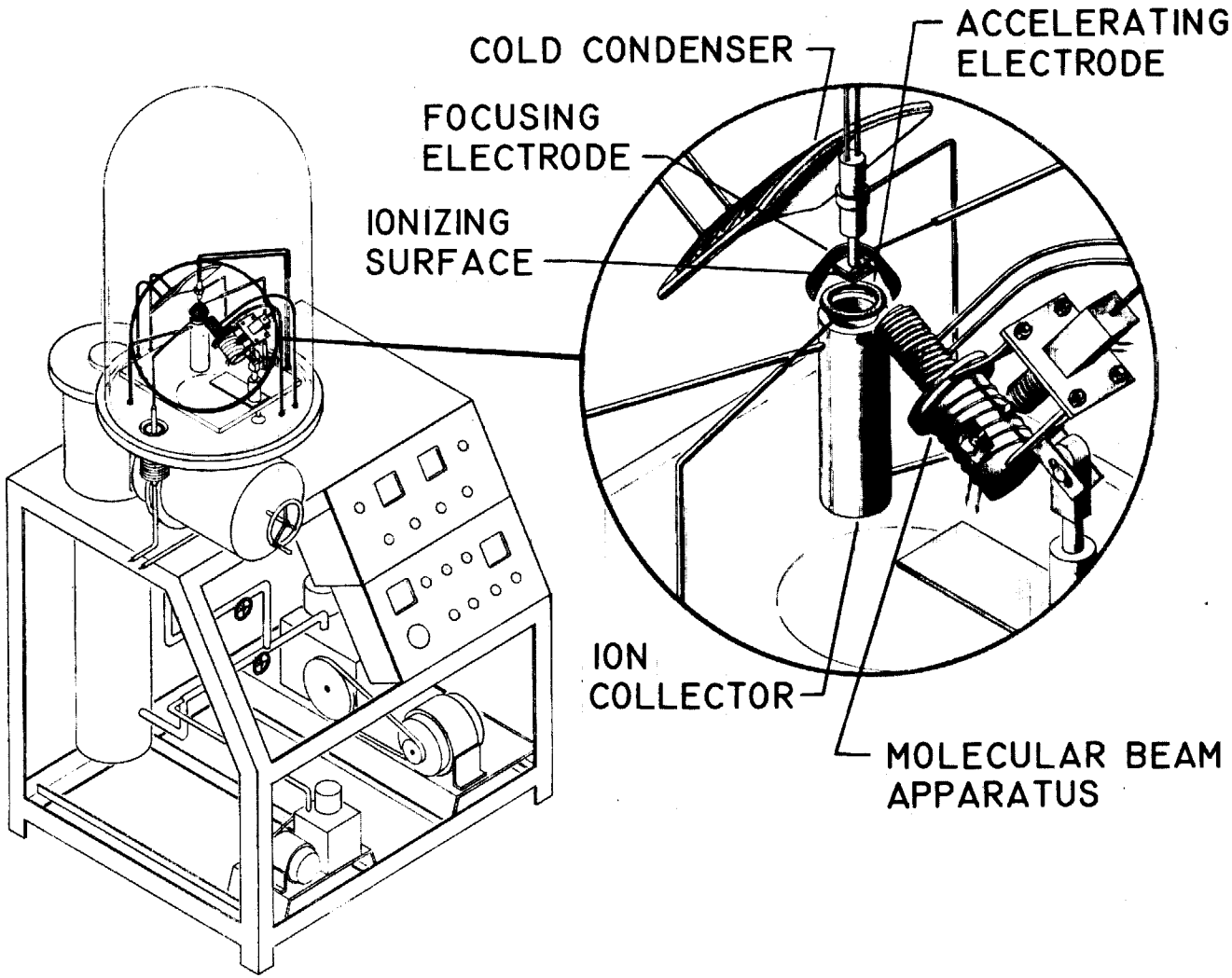

(b) Diagram of apparatus.

Figure 13. - Concluded. Apparatus for surface ionization studies.

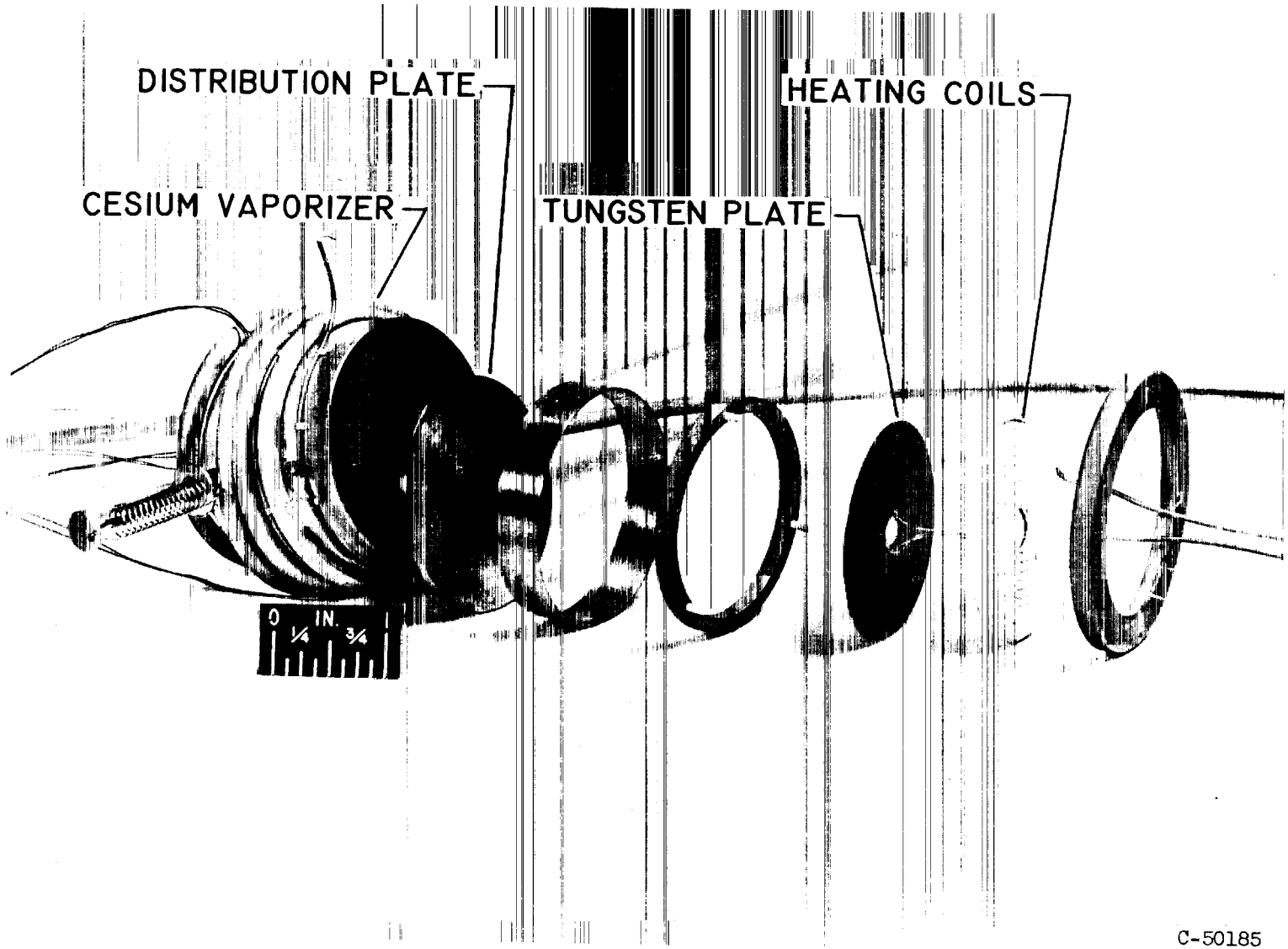

Figure 14. - Apparatus for measuring current density from a hollow ion source.

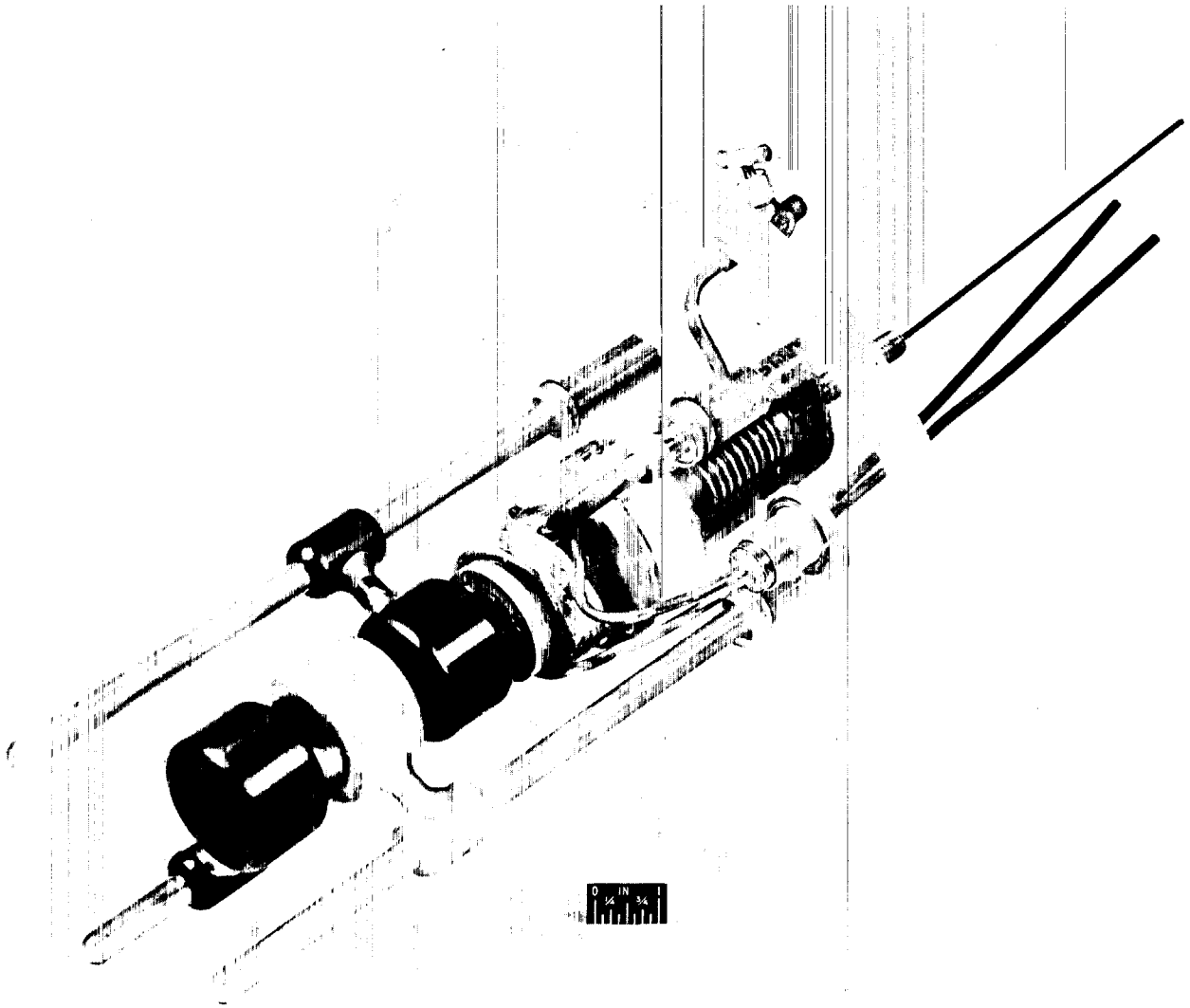

C-49334

(a) Photograph of apparatus.

Figure 15. - Electric arc ion source.

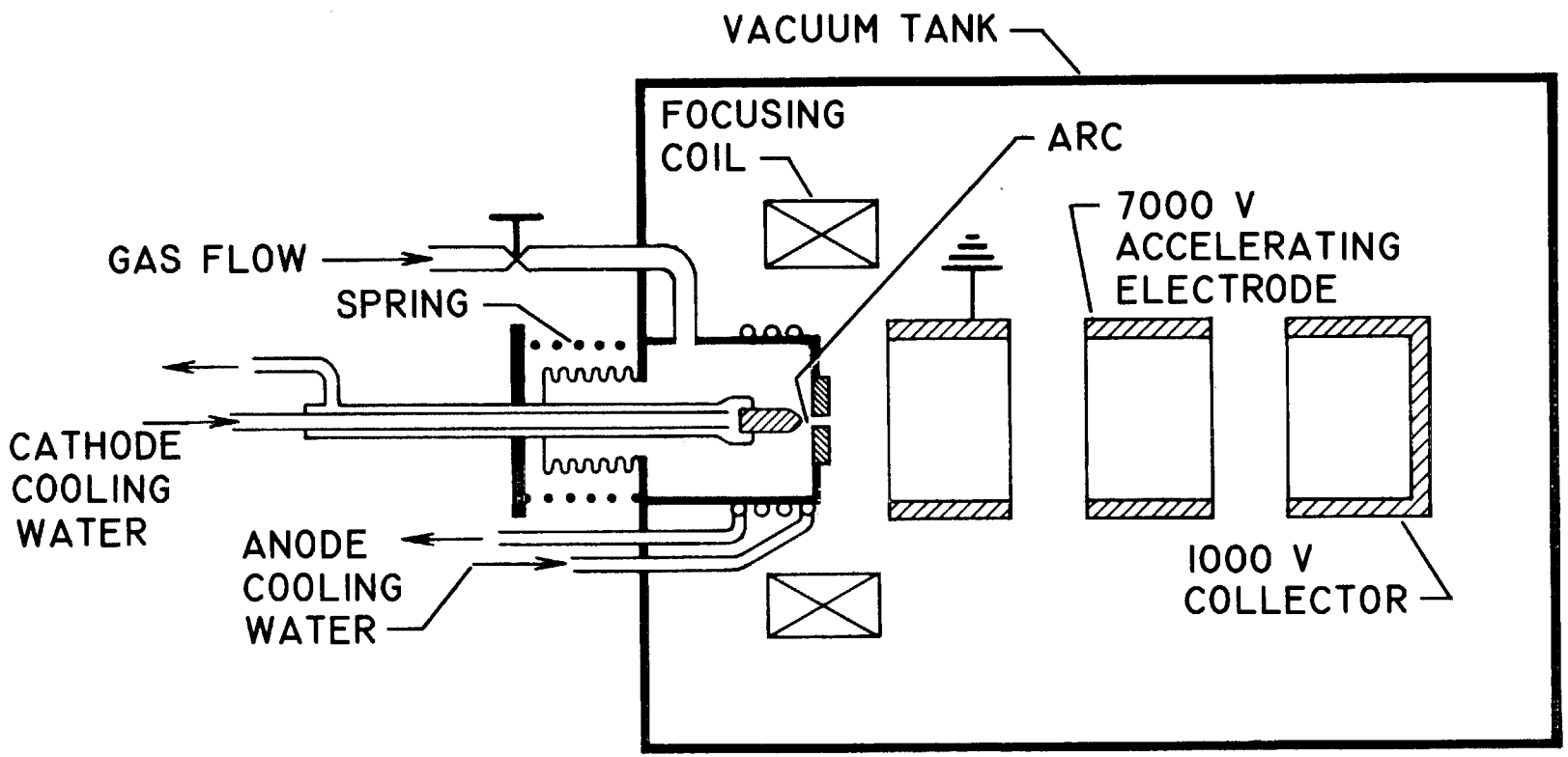

(b) Diagram of apparatus.

Figure 15. - Concluded. Electric arc ion source.

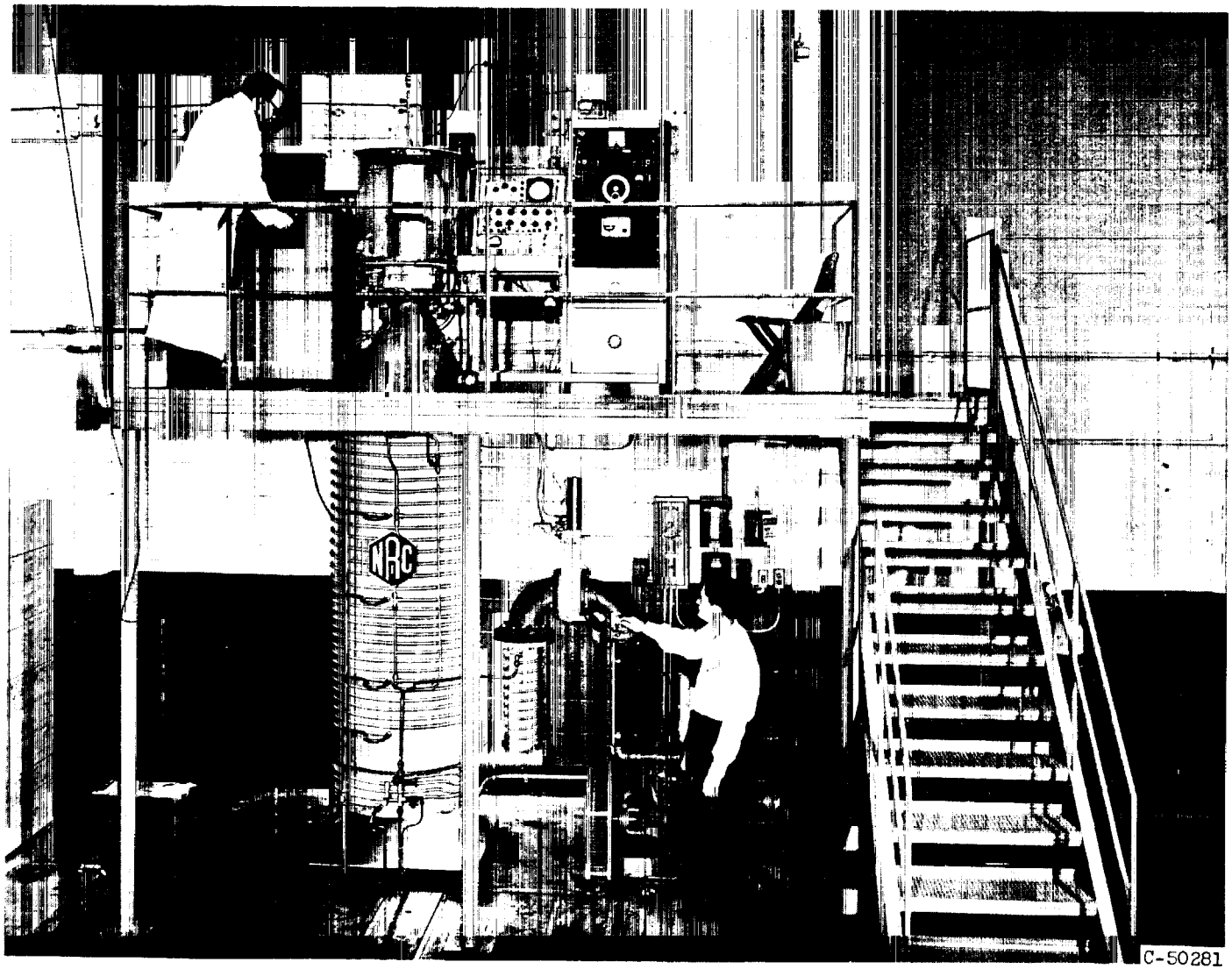

Figure 16. - Apparatus for studying ionization by RF heating.

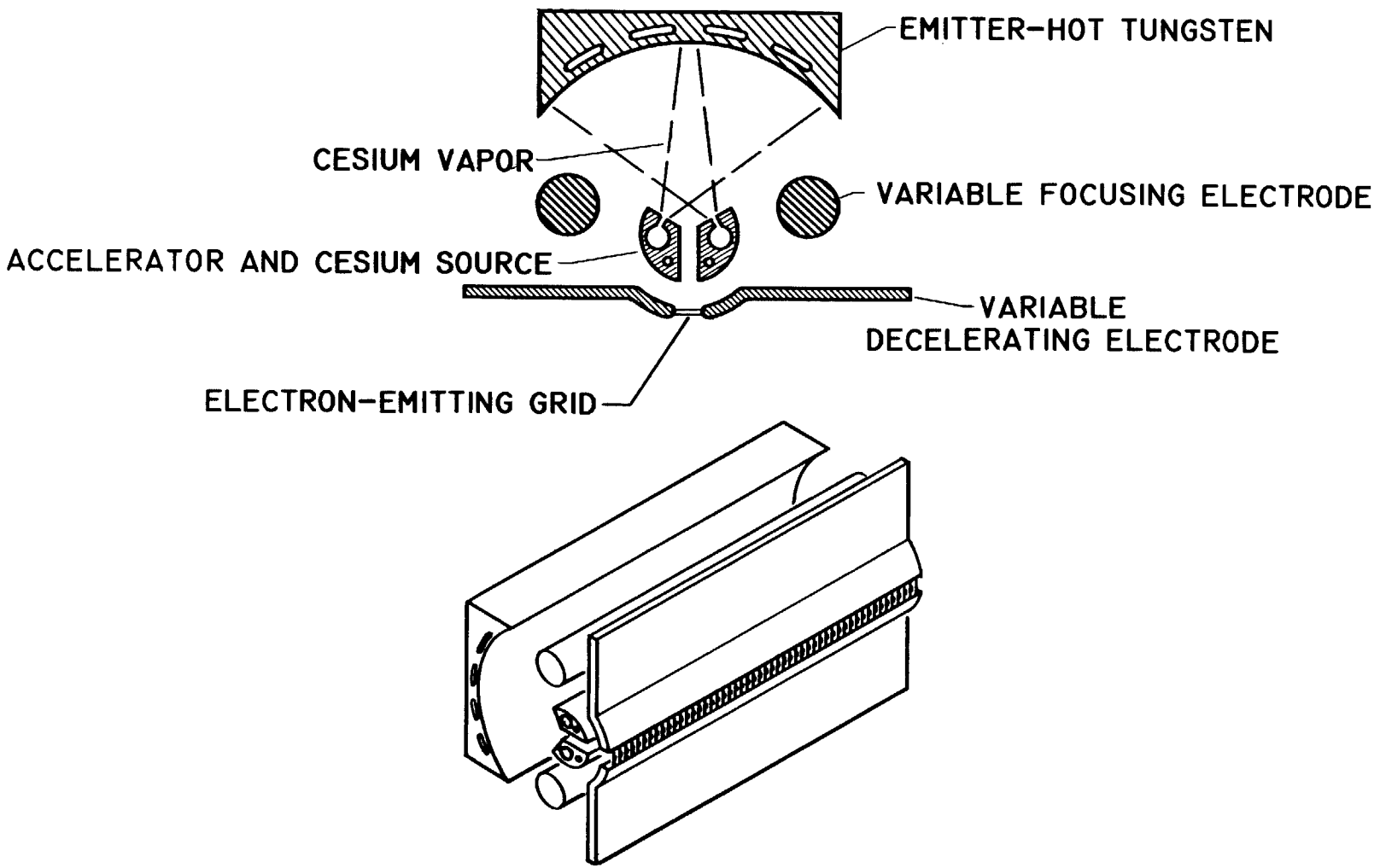

Figure 17. - Strip beam ion accelerator designed after high-perveance electron guns of reference 8.

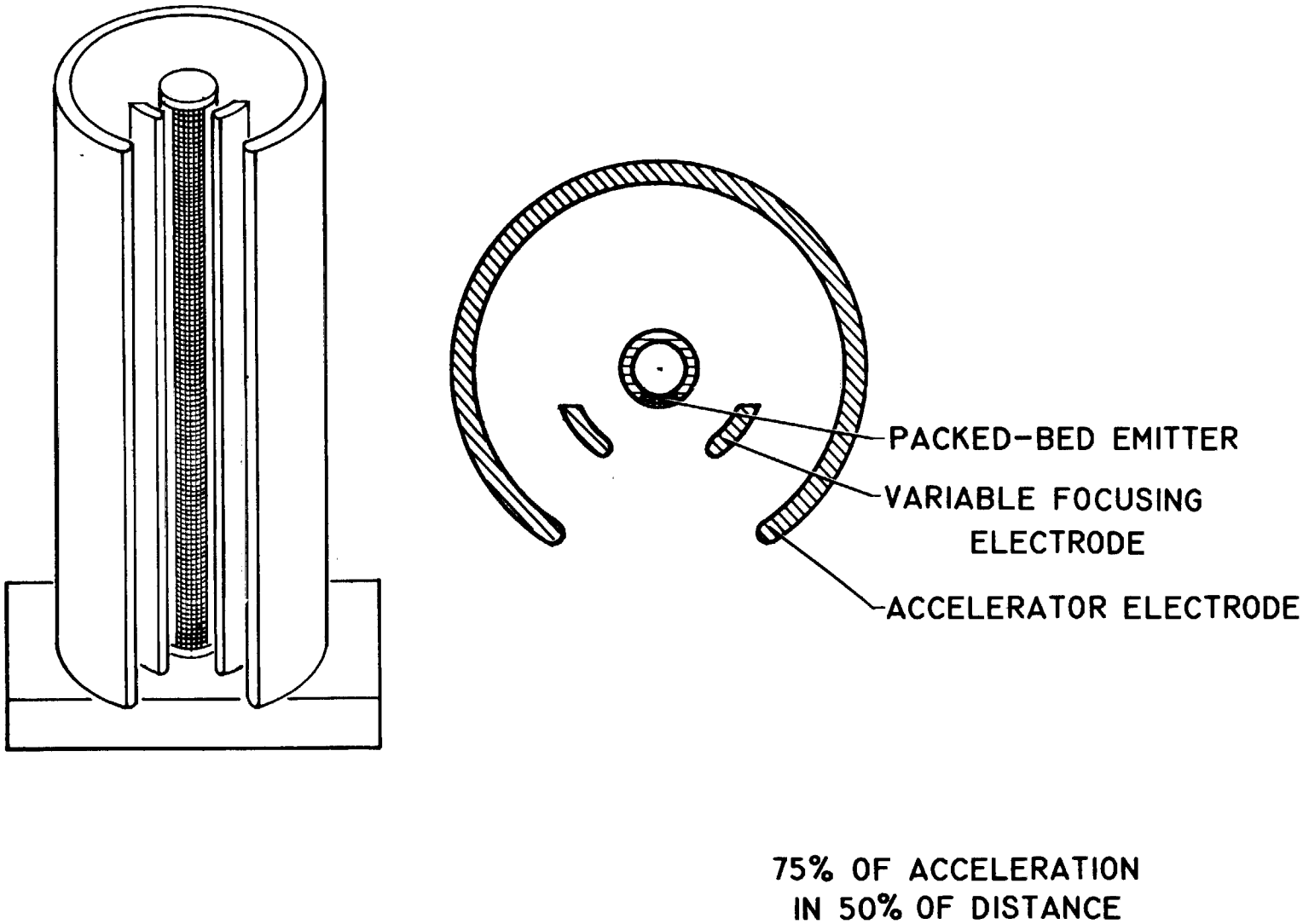

Figure 18. - Strip beam ion accelerator with ion emission from inner cylindrical surface.

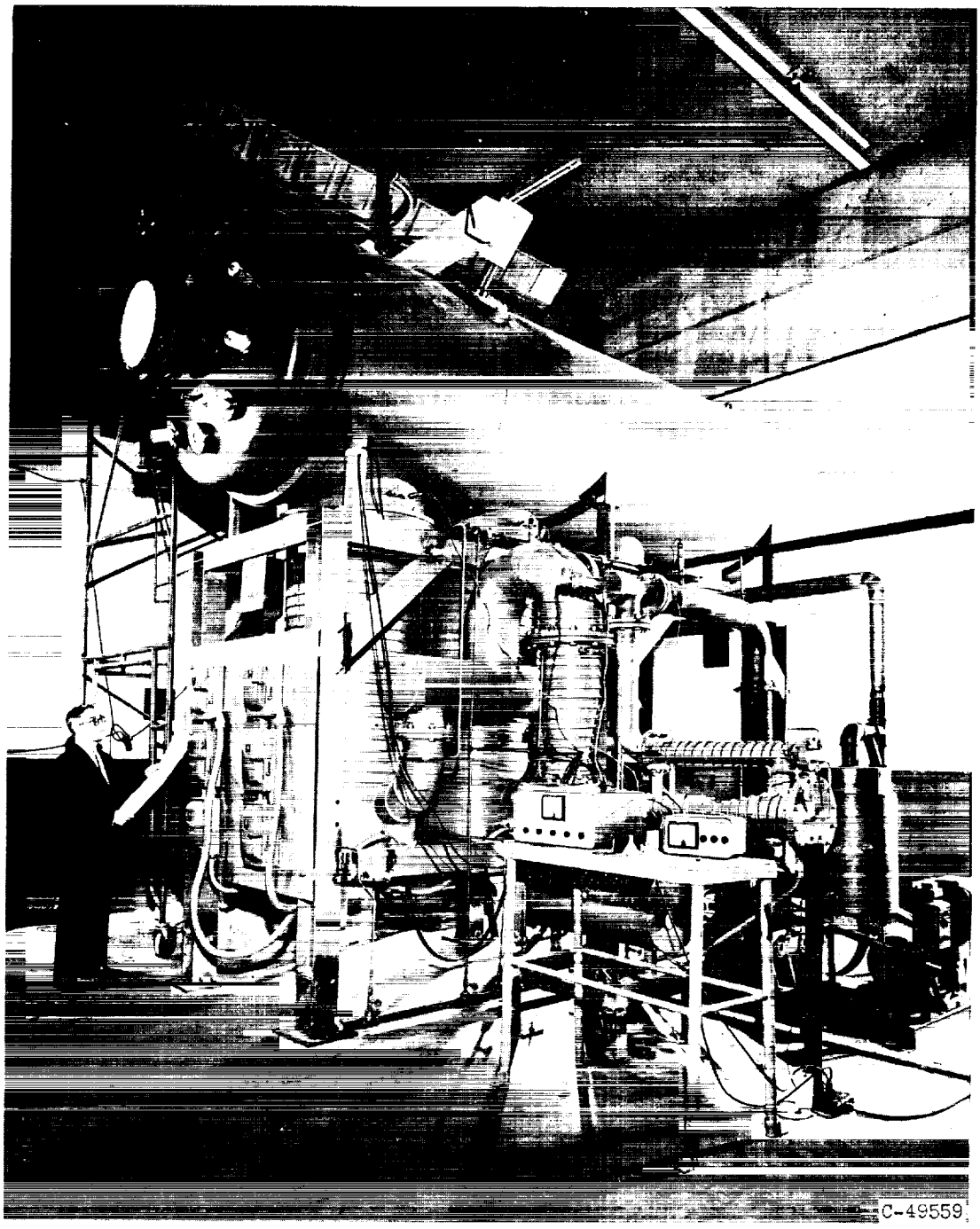

(a) Photograph of facility.

Figure 21. - Ion rocket test facility.

E-453

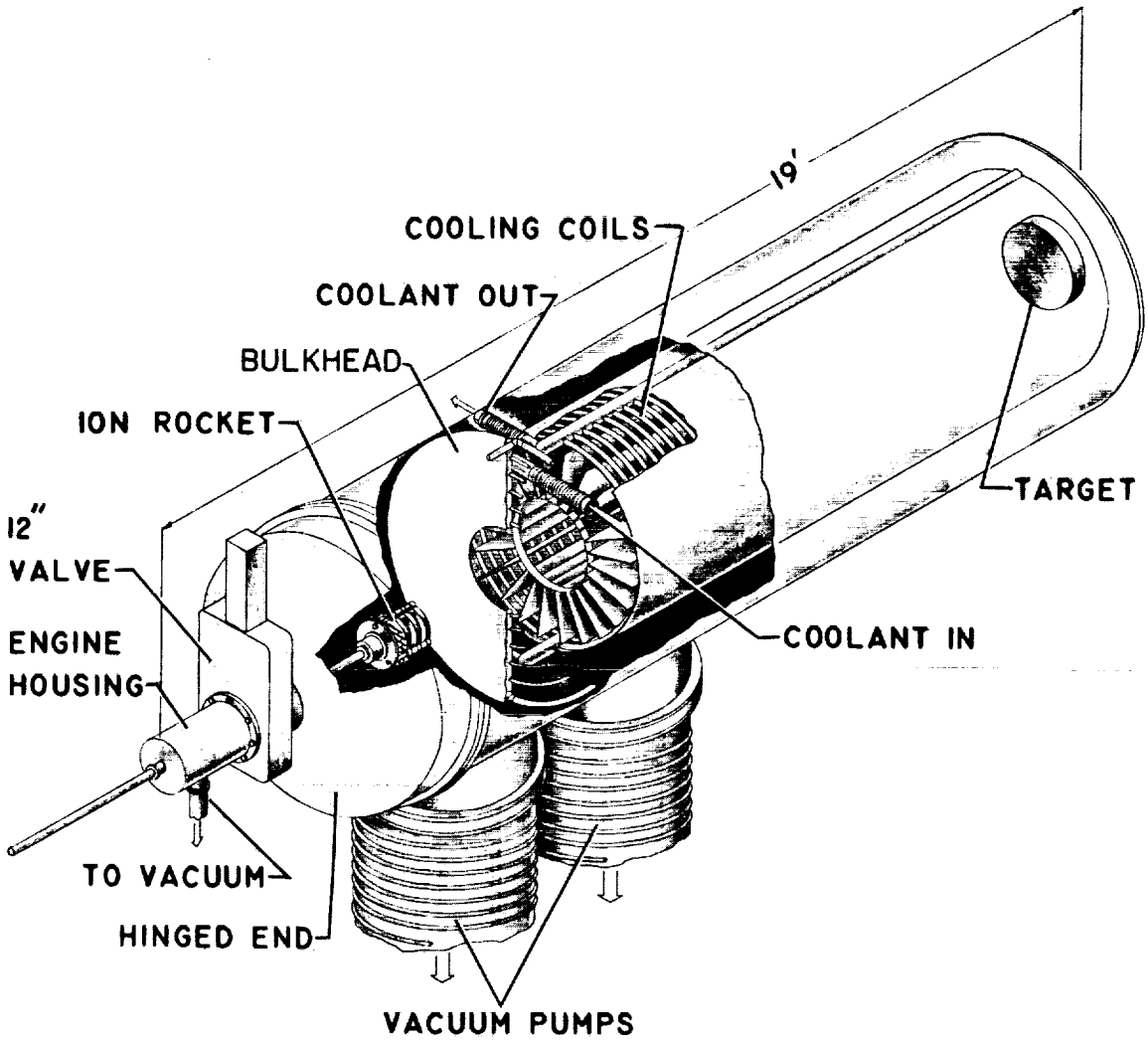

(b) Cutaway drawing of facility.

Figure 21. - Concluded. Ion rocket test facility.

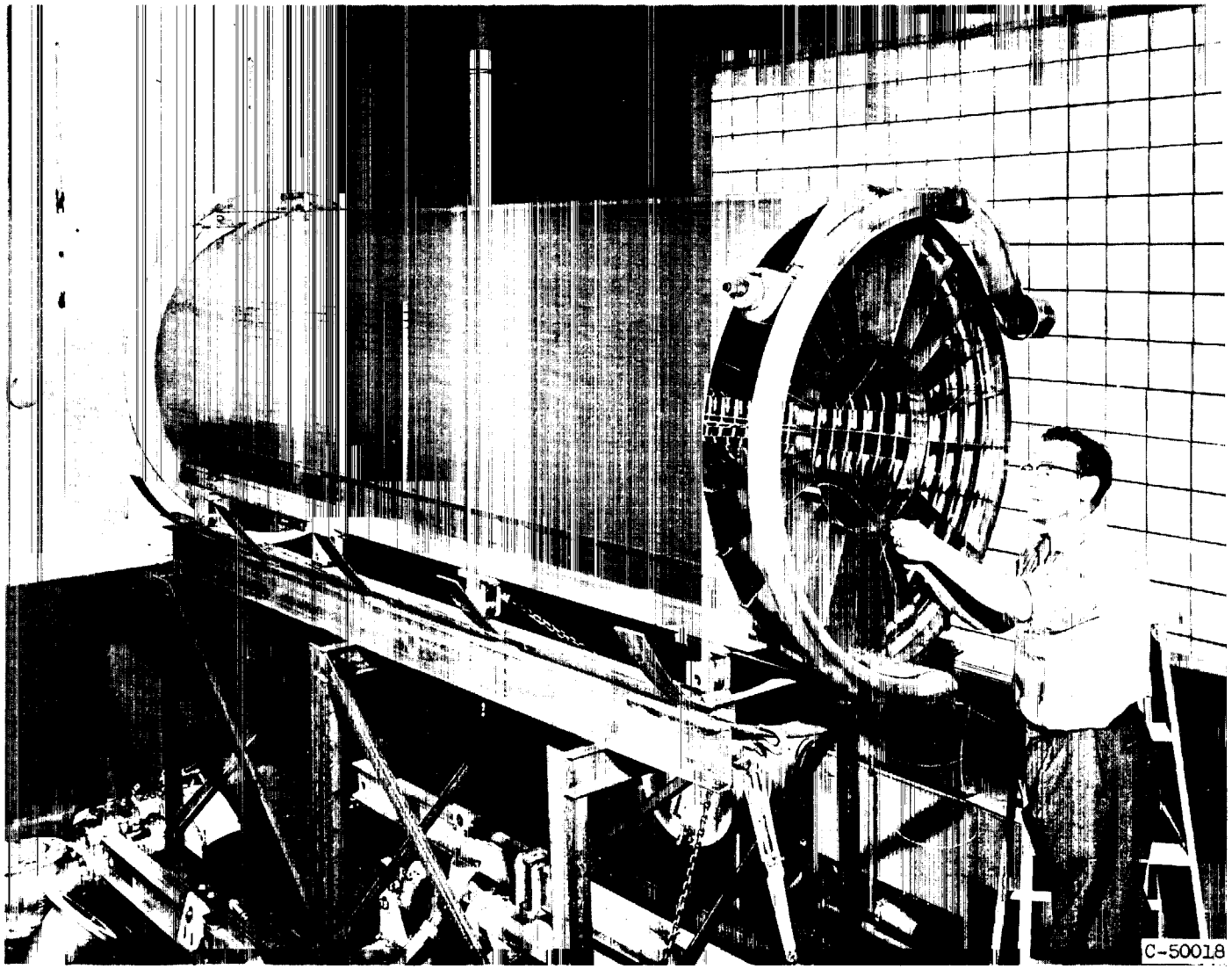

Figure 22. - Condenser baffles from ion rocket tank.

E-453

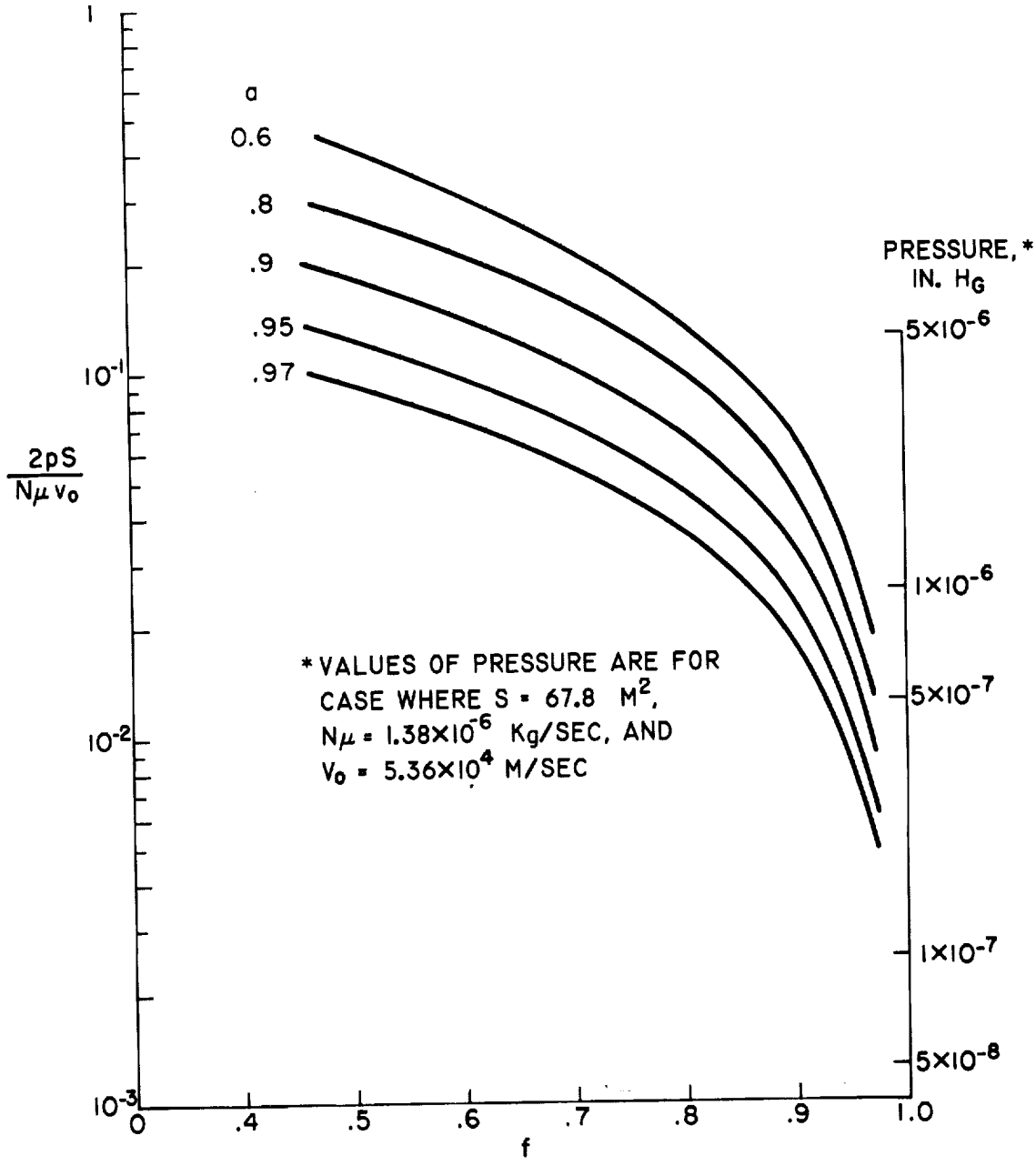

Figure 23. - Condenser performance for various accommodation and sticking coefficients.